2016

Integrated Tandem Dye Sensitized Solar Cell (DSSC)-Lithium Ion Battery

Geetha Varnekar
South Dakota State University

INTEGRATED TANDEM DYE SENSITIZED SOLAR CELL (DSSC)-LITHIUM ION BATTERY

BY

GEETHA VARNEKAR

A thesis submitted in partial fulfillment of the requirements for the

Master of Science

Major in Electrical Engineering

South Dakota State University

2016

INTEGRATED TANDEM DYE SENSATIZED SOLAR CELL (DSSC)-LITHIUM ION BATTERY

This thesis is approved as a creditable and independent investigation by a candidate for the Master of Science degree and is acceptable for meeting the thesis requirements for this degree. Acceptance of this thesis does not imply that the conclusions reached by the candidate are necessarily the conclusions of the major department.

Qiquan Qiao, Ph.D. Date

Thesis Adviser

Steven Hietpas, Ph.D. Date

Head, Department of Electrical

Engineering and Computer Science

Dean, Graduate School Date

ACKNOWLEDGEMENTS

The work presented in this thesis was supported by NASA EPSCoR (Award #: NNX14AN22A), and by the State of South Dakota.

First and foremost, I would extend my deepest gratitude to Dr. Qiao as my supervisor and graduate coordinator for providing me the opportunity of working in his research group as a research assistant and his enormous help throughout this project and for his valuable suggestion and continuous encouragement has helped me to carry out my research successfully.

I am grateful to Dr. Yoon and Dr. Huitian Lu for their important role as my research committee member by providing interesting and timely suggestion. I express my sincere thanks to all my friends, especially Ashim Gurung, in helping me to carry out my experiment.

I wish to thank all my teachers at Electrical Engineering department of SDSU for imparting knowledge to carry out their support throughout.

Finally, I would like to thank my family for continues support, love, encouragement and keeping me always motivated to learn and grow.

TABLE OF CONTENT

LIST OF FIGURES

LIST OF TABLES

ABSTRACT

INTEGRATED TANDEM DYE SENSITIZED SOLAR CELL (DSSC)-LITHIUM ION BATTERY

GEETHA VARNEKAR

2016

Efficient renewable energy harvesting and storage are needed for present challenges related to clean environment and increasing energy demand. Different types of energy harvesting technologies such as solar, thermal and wind require excess energy to be stored in batteries, which further adds to the complication and increase in cost to the overall renewable energy system. Integrating the generation and storage of solar energy in a single device would be a more cost effective way towards meeting the increasing energy demand due to its simplicity in design and less space consumptions. Herein, a sustainable photovoltaic cell integrated with an energy storage device was developed that addresses short term photovoltaic (PV) power variability using dye sensitized solar cell (DSSC) in a tandem structure with thin film based lithium-ion battery. As lithium based batteries have been addressed as efficient charge storage system due to its high energy storage density and extended lifecycle performance. The integrated structure uses a common anode (titanium foil coated with anatase TiO_2 on both sides which serves as DSSC and lithium ion battery anode) which showed an open-circuit voltage of ~3 V, a short circuit current density of ~40mAhg^{-1} and a storage efficiency of ~0.80%. This new device can serve as power source to mobile storage applications.

Chapter 1 : Introduction

1.1 Background

After World War II baby boom crisis, there has been a drastic increase of population which leads to huge energy demand. This has directed mankind to widely use fossil fuels like oil and gas which leads to increase in pollution and greenhouse effect and being a major cause of global warming [1]. According to renewables 2016 global status report, by the end of 2015, non- renewable energy shared 76.3% of global electricity production and renewable energy shared rest 23.7% in which 3.7% by wind, 2% by bio-mass, 1.2% solar PV and 0.4% geothermal and oceans as shown in Figure 1.1 [2] According to NASA report on climate change due to global warming and greenhouse effect which leads to increase in globe temperature, highest globe temperature was found on August 2016 which was increase in 1.76°F (0.98°C) and was recorded as the hottest year on earth from 1880 and this is caused due to emission of greenhouse gases to the earth's atmosphere[3]. As this effect lead on lack of oxygen and fresh air, around 6.5 million premature deaths occur every year due to air pollution caused by combustion of fossil fuels as per the World Energy Outlook Special Report 2016 energy and air pollution [3]. The researches predicted obsolete of non-renewable energy resources. Hence, a new alternative pollution free renewable energy source is required to meet the world energy needs.

The worldwide recognized abundant and pollution-free energy source is solar energy in which the earth receives about 174 petawatts of solar radiation at the upper atmosphere, out of which 30% is reflected to space and the remaining is absorbed by the

earth's atmosphere, oceans and land masses [4]. This realization has directed in huge interest on solar energy harvesting for many applications as power generators, solar heaters and transports.

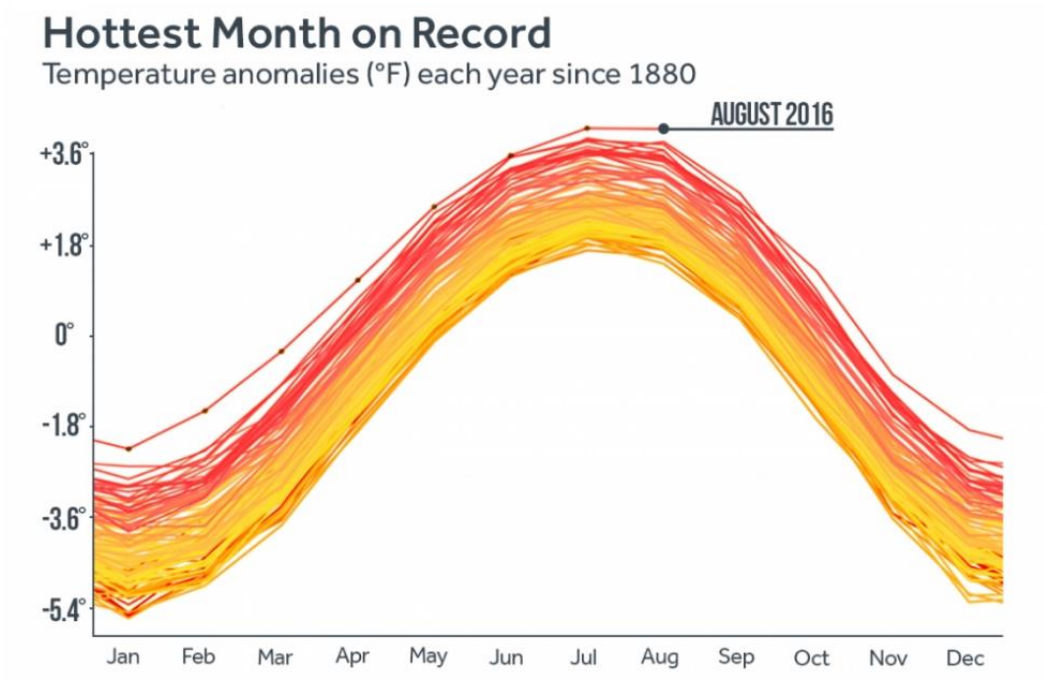

Figure 1.1. Global temperature raise from 1880 to August 2016 due to global warming [3]

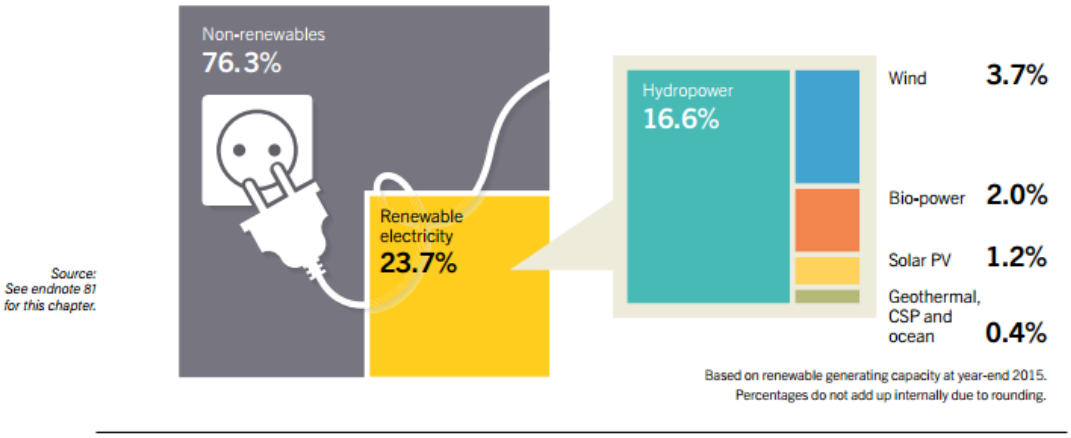

Figure 1.2. Estimated renewable energy share of global electricity production, End-2015 [2]

According to renewables 2016 global status report. The forecast of the year 2010 through 2015 shows, solar photovoltaics (PV) technology gained huge attention, and recognized as the fastest growing renewables. Solar PV total global capacity has been exponentially increased in which by end of 2015, around 227 Gigawatts of electricity was generated using PV technology as shown in Figure 1.3 [2].

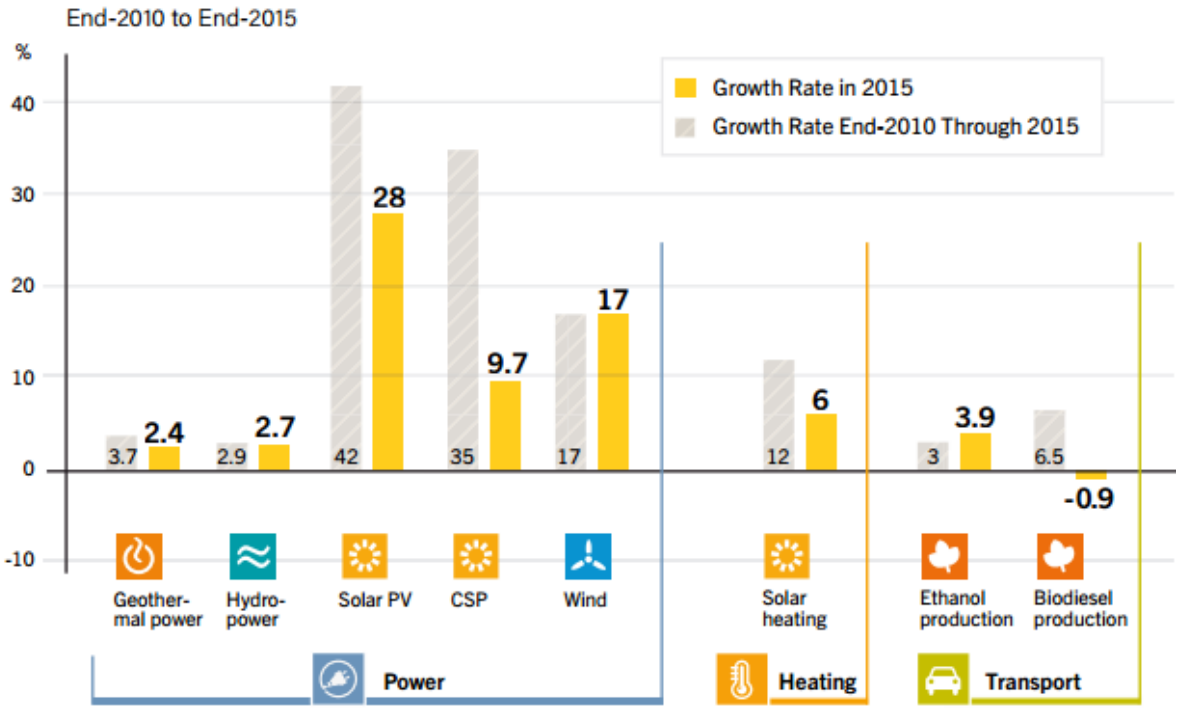

Figure 1.3. Average annual growth rates of renewable energy capacity and biofuels production (2010-2015) [3]

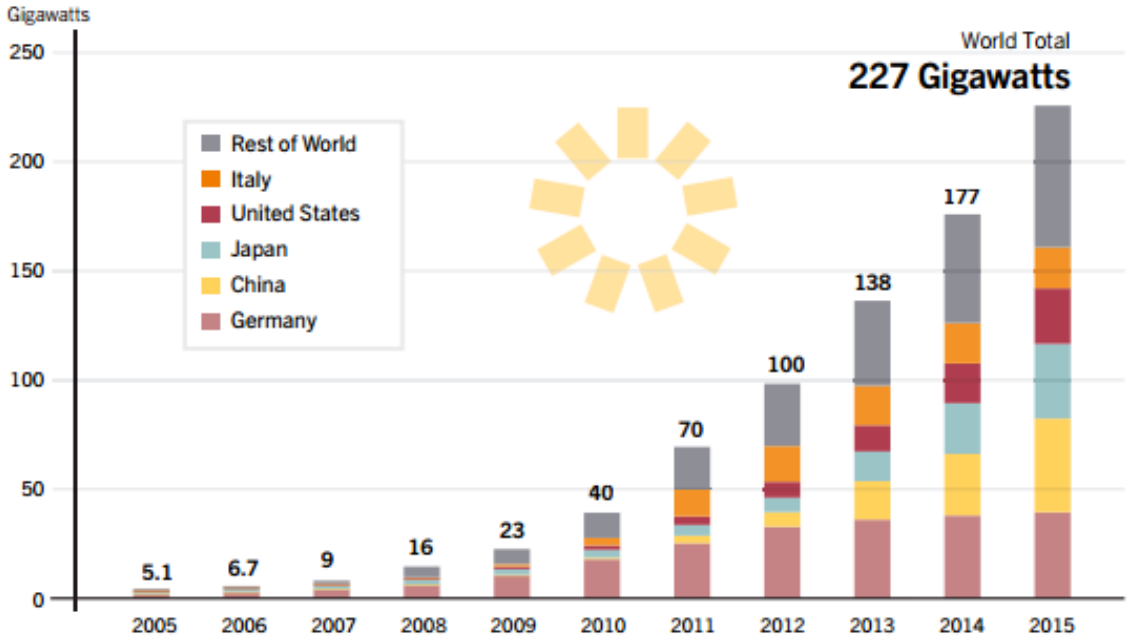

Figure 1.4. Solar PV total global capacity as per end of 2015 [2]

Silicon has been identified as the most efficient material to generate electricity by converting solar energy into electricity [5]. The solar panels are connected either in series or parallel to produce electricity. But the major drawback of PV is the inconsistency of solar irradiation due to clouds, climatic change and long day night effects [6] which leads to high PV power fluctuations.

Combination of hydropower generators and PV has proven that PV can generate power in the day time and hydropower can be consumed when the solar power is not available [8]. This process can support irrigation and power supply to wide areas but was still found hard to meet the demands due to its slow response time and system complexity. Table1 shows the different storage and power generation methods with their response time that are being currently used.

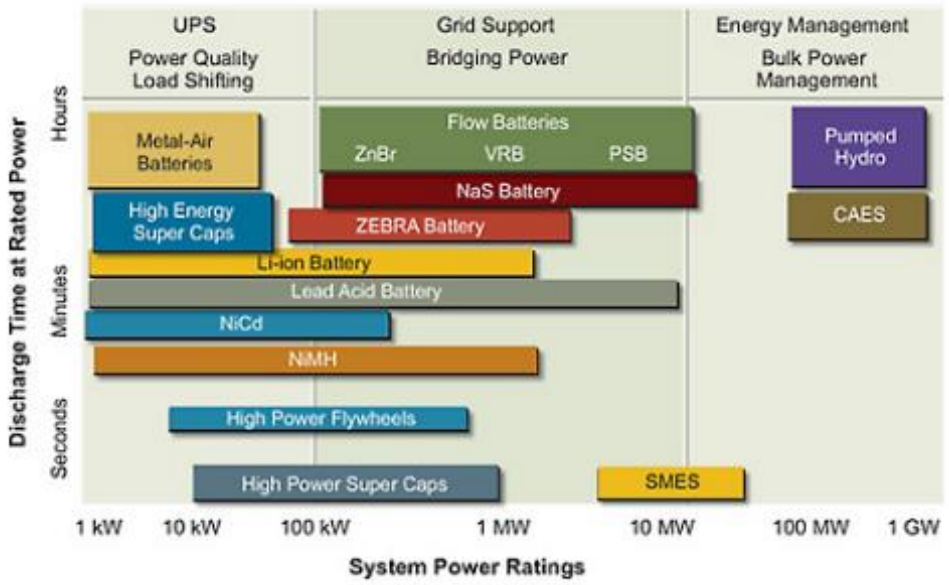

Figure 1.5: Types of power generation and power rating [9]

Table 1: Types of power generation and storage

Technology	Response Time	Cycle Life	Efficiency	Storage Capacity	Cost per kWh (10 years)
Flywheels	Seconds	Very high	>90%	100 kW+	$300 – $800
Battery	Seconds	Low	Variable	kW	$150-$800
Hydro	Minutes	Moderate	70-85%	MWs	$45-$90

1. Flywheels are found promising due to its high cycle life, greater efficiency but limited by cost to produce high power and hence low cost solution should be introduced.
2. Hydro has high storage capacity and cheaper, but limited by slower response rate.

3. Batteries have faster response rates but its power efficiency and cycle life are limited and are difficult to physically connect with PV due to bulky nature [9].

Therefore, an investigation on integration of batteries with PV on a single unit could effectively reduce cost and overcome the bulky nature on using all different techniques and improves the practicality of using PV power generation.

1.2 Literature Review

The first integration pack of PV and battery was proposed by Miyaska et al. in 2005 [11] in which a three-electrode system dye sensitized photo-capacitors were used as shown in figure 1.5 [11]. The battery was charged at 0.8V in 3 minutes under 100mWcm^{-2} with a reported energy density of 47 μAcm^{-2} with **coulombic efficiency 42%** and capacitance 0.65 Fcm^{-2}. But this study was limited to its control due to switching of electrodes consumes extra energy and increases cost of fabrication.

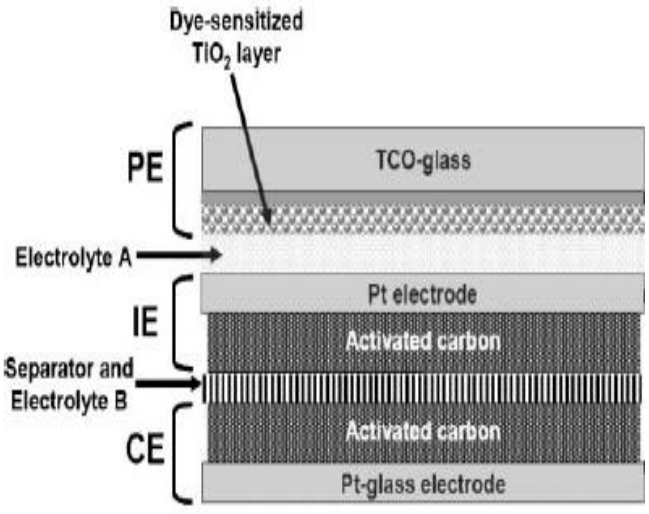

Figure 1.6. Structure of the three electrode dye sensitized photo capacitor [11]

An all-solid state integrated device was developed using free standing and aligned multi-walled carbon nanotube (MWCNT) films as electrodes as shown in Figure 1.10 [14] by Z. Yang et al. in 2013[14]. The integrated device was charged to 0.72 V in 8 Seconds under 100 mW 1.5 AM solar illumination. With **reported efficiency of 6.1%** and galvanostatically discharged to 0 V in 35 seconds with **coulombic efficiency of 84%** and **photoelectric conversion and storage efficiency 5.12%.** The integrated device which incorporated polyaniline into MWCNT film was charged in 33 seconds and galvanostatically discharged to 0 V in 2.5 minutes which obtained coulombic efficiency 70% and entire photoelectric conversion and storage efficiency 4.29%. Also a flexible integrated device was fabricated which showed charge time ~3 minutes, discharge time ~2.5 minutes @ 1.4 $mAcm^{-2}$, specific capacitance 83 Fg^{-1}, coulombic efficiency 34% and entire photoelectric conversion and storage efficiency 0.79%.

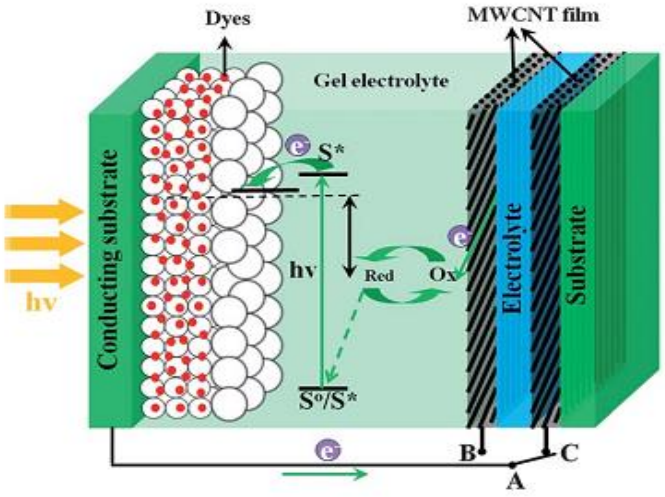

Figure 1.7. Schematic illustration of an integrated device based on aligned MWCNT films as electrodes [14]

Photovoltaically self-charging cell was realized by modifying counter electrode of DSSC with Pt/Au/PVDF/ZnO nanowire composite was reported by. Zhang et al. 2013 [12]. It was reported that two electrode system with high dielectric constant of PVDF and high surface area of Nano-materials were used, with achieving **solar cell efficiency of 3.7%** and solar charge density of 2.14 Cg^{-1} and stored energy density 1.4 $mWhkg^{-1}$ However, only a part of photo generated electrons are used for storage which is a typical operation of super capacitors. Hence, requires a storage with higher energy density to generate continuous power output. But gel electrolytes relatively has slower response rate that leads to delay in switching performance of the PV and battery and underlying physical principles are critical in solid state devices.

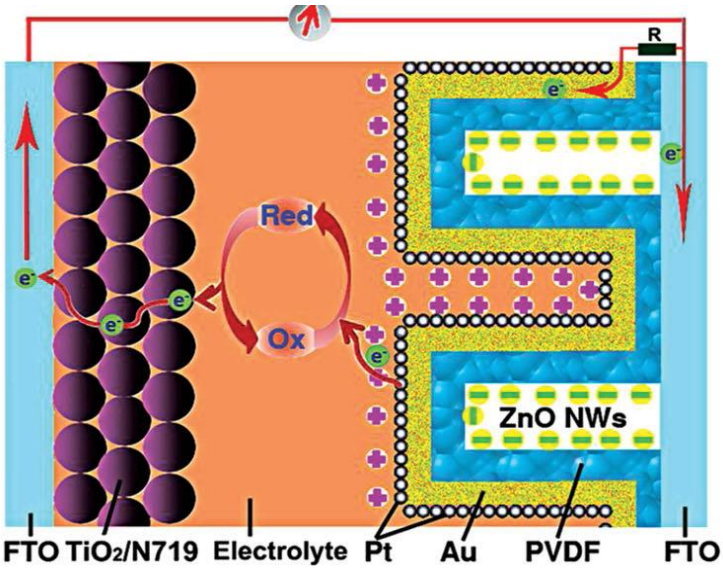

Figure 1.8. Schematic structure of DSSC with modified counter electrode [12]

An integrated power pack of DSSC and lithium ion battery was reported. By Guo et al. in 2012 [13] in which the Tandem DSSC and li-battery both use the same Titanium foil that has double sided Titanium dioxide nanotube arrays as shown in the figure 1.7

[13]. The reported charge capacity was 3V in 8 minutes with a discharge capacity of 38.89 μAh for discharge of 100 μA with **total energy conversion and storage efficiency of 0.82%**. But the paper was limited to description of underlying physical principles of the working of integrated device and information on charge/discharge control. The efficiency would require a higher energy storage density and performance of device under intermitted illumination need to be performed. However, the tandem structure in the solar cell would make complexity in fabrication and mismatch in red-ox potentials of the battery.

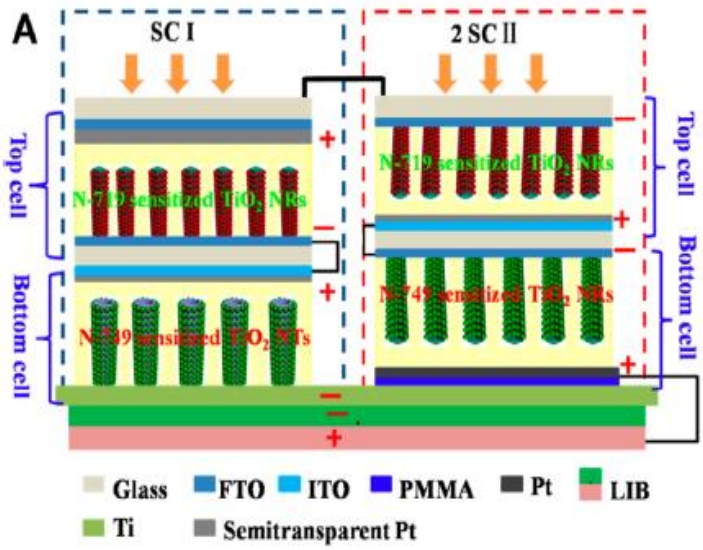

Figure 1.9. Integrated structure of Tandem DSSC and Lithium ion battery [13]

1.3 Motivation

There is a need for cost effective and sustainable PV with energy storage that addresses short term PV power variability is needed.

1.4 Objective

Investigate energy storage systems for PV to achieve cost effective and reduced resign complexity by engineering simple photovoltaic energy harvesting by integrating

DSSC, as a solar cell and Lithium ion battery, as a storage device and ultra-low power boost converter to charge the battery by:

1. Fabricate and study the behavior of coin cell and thin film based half-cell and full cell Battery.
2. Fabricate and study the behavior of transparent counter electrode DSSC for rear illumination on integrated device.
3. Fabricate and study the behavior of coin cell lithium ion battery and physically connect to the commercial solar cell and characterize the charge-discharge criteria using a boost converter.
4. Integrating single DSSC and Li-ion full cell battery using a common titanium foil based electrode.

Chapter 2 : Theory

2.1 Solar Cell Operation

Solar cells are the type of optically and electrically conducted cells which converts absorbed light into electrical energy which behaves like a simple p-n junction.

2.1.1 p-n Junction

Electrically conductive metal where the electron flow takes place is typically called a p-n junction. Silicon is an intrinsic metal and these type of pure metals are non-conductive hence an impurity/dopant must be added to make them conductive to maintain the energy bandgap for flow of electrons. Bandgap is nothing but the energy level difference between valance band and conduction band of a material as shown in the figure 2.1. Phosphorous is used as electron donor which is an n-type material and boron is used as an electron accepter which is a p-type.

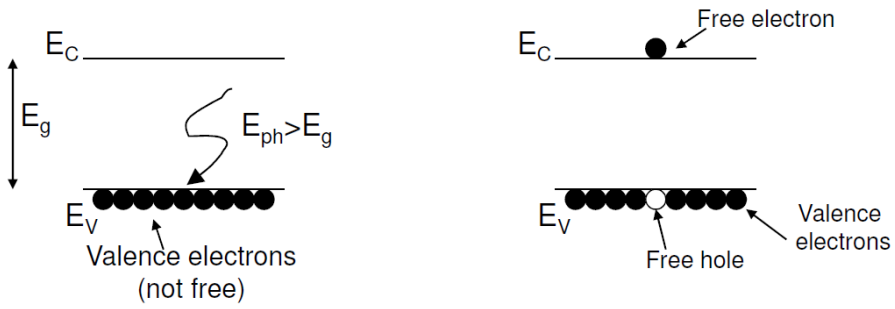

Figure 2. 1. Photoexcitation in semiconductors– modified from [17]

A solar cell typically consist two dopant materials (p-n materials) which bought in physical contact by making a P-N junction. Figure 2.2 shows operation of a p-n junction.

This physical contact creates a concentration gradient for electrons and holes which leads to diffusion of electrons in p and holes in n which produces current density for electrons Jn,diff, and holes, $J_{p,\,diff}$, are described by [15]

$$J_{n,diff} = qD_n \frac{dn(x)}{dx}, J_{p,diff} = -qD_p \frac{dp(x)}{dx} \quad (2.1)$$

where, q is the electron charge, Dn and Dp are the diffusion coefficients for electrons and holes, n and p are the electron and hole concentrations.

These diffused electron enter p-side and recombines with holes near the junction and diffused holes enter n-side and recombines with electrons. As the free charge carriers become low/depleted at the junction called depletion region [16]. Hence, this leads to an internal electric field to form positive and negative ions called Gauss law. This electric field counteracts the diffusion by drifting holes towards the p-side and electrons towards the n-side. Drift current density for electrons (Jn) and holes (Jp) are [16]:

$$J_n = qn\mu_n E\ , \quad J_p = qp\mu_p E \quad (2.2)$$

Where, μn and μp are the mobility of electrons and holes, E is the applied electric field intensity. This process continues until equilibrium is reached.

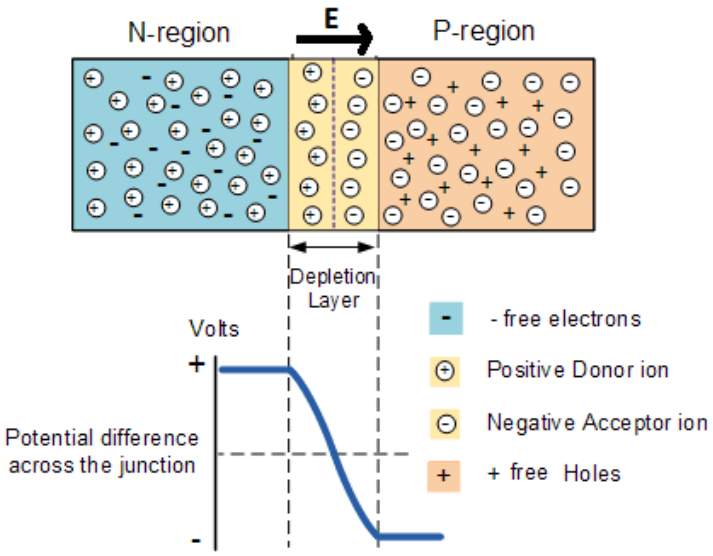

Figure 2.2. Structure of a p-n junction– modified from [16]

2.1.2 p-n Junction under Illumination

The illuminated p-n junction structure is as shown in the figure 2.3. With the presence of light, material absorbs photons and electrons are excited in valance band to conduction band forming an electron-hole pair at the junction [16]. Energy of photon (E) can be determined in following equation:

$$E = h\upsilon = \frac{hc}{\lambda}\ (in\ joules) = \frac{1.24}{\lambda}\ (in\ eV) \tag{2.3}$$

Where, h is the Planck's constant (6.63 × 10-34 J-s), υ is the frequency of photon in Hertz, c is the speed of light (2.998 × 108 m/s) and λ is the wavelength of the photon in meters.

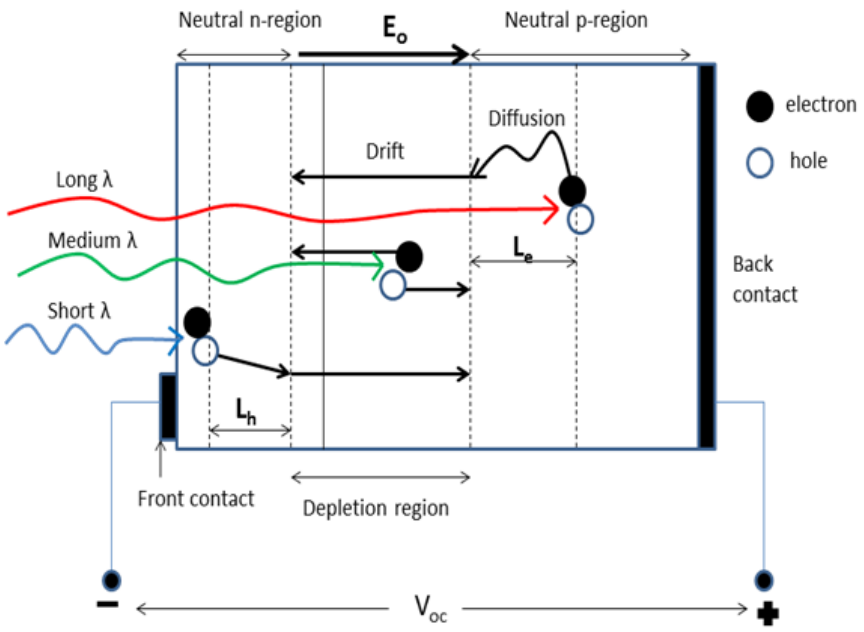

Figure 2.3. Electron-hope pair during illumination – modified from [16]

Figure 2.4. Shows the electrical equivalent circuit of the solar cell and the current responses [15]. The built in electric field sweeps electrons towards the n-side and holes towards p-side. These free charge carriers become excess majority carriers and produce current in the external circuit. This is called photocurrent (Iph) or short circuit current (Isc) which is proportional to the intensity of incident solar radiation (I). When the device is connected to an external load, a voltage appears across the junction which creates current flowing in opposite direction to Iph [15]. This current is called forward diode current (Id) which is expressed as [15]:

$$I_d = I_o[\exp\left(\frac{eV}{\eta kT}\right) - 1] \tag{2.11}$$

Where, Io is the reverse saturation current, η is the ideality factor (ranges from 1 to 2), e is the elementary charge, k is the Boltzmann constant and T is the temperature in Kelvin.

The net current flow in a solar cell is therefore expressed as:

$$I = I_d - I_{ph} = I_o \left[\exp\left(\frac{eV}{\eta kT}\right) - 1\right] - I_{sc} \tag{2.12}$$

The open circuit voltage, Voc, can be obtained when I is set to zero as:

$$V_{oc} = \frac{kT}{e}\ln\left(\frac{I_{sc}}{I_o} + 1\right) \tag{2.13}$$

Other performance parameters that define a solar cell are fill factor (FF) and efficiency (η). FF measures the closeness of the real I-V curve to the ideal rectangular shape and is expressed as [1]:

$$FF = \frac{I_m V_m}{I_{sc} V_{oc}} \tag{2.14}$$

Where, I_m is the current at maximum power point and V_m is the voltage at maximum power point. Efficiency is the ratio of output electrical power density to input power density, P in, which is defined as [15]:

$$\eta = \frac{P_m}{P_{in}} = \frac{I_{sc} V_{oc} FF}{P_{in}} \tag{2.15}$$

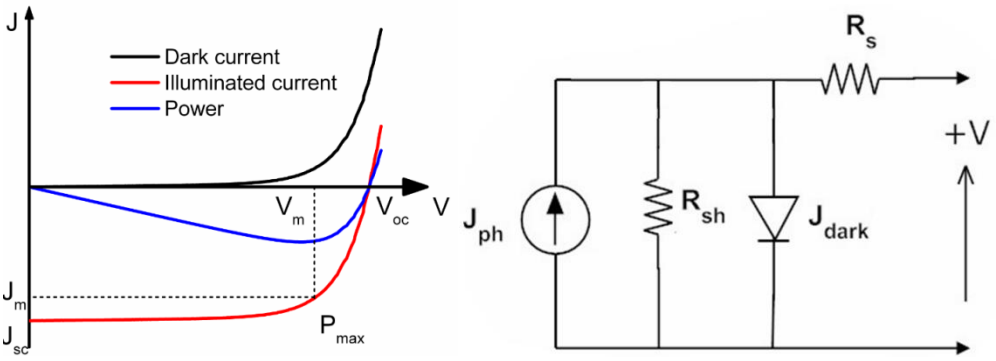

Figure 2.4 (a) Typical J-V curves of a solar cell in dark and illumination; (b) equivalent circuit for a solar cell– modified from [15]

During minority carrier lifetime τ_m, that is the time taken for electrons and holes to reach the junction and the maximum distance to travel before recombination called minority carrier diffusion length, Lm, which can be given as:

$$L_m = \sqrt{D_m \tau_m} \tag{2.10}$$

Where, Dm is the diffusion constant and m is the electrons or holes.

2.1.3 Types of Solar cells

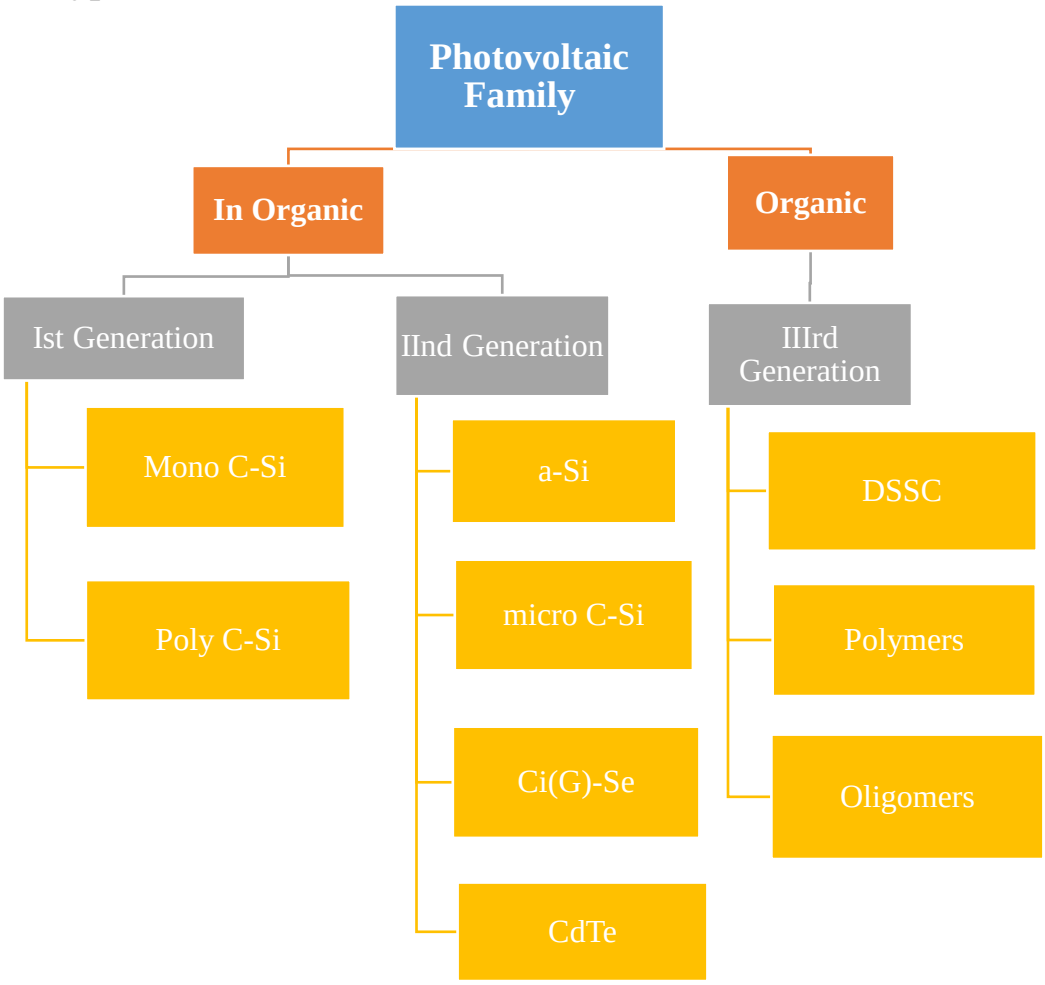

Figure 2.5 Overview of Photovoltaic Technology-modified from [27]

Figure 2.5 shows the photovoltaic technology of In Organic and organic types for technology enhancement and environmental improvements [27].

Table 2. Differences between Organic and In-Organic solar cells – modified from [27]

Properties	Inorganic (e.g. Si)	organic (e.g. Polymer)
Absorption coefficients	10^3-10^4 cm^{-1} (500-800 nm)	high (>10^5 cm^{-1})
Optical band gap	1.12 eV for Si	~ 2 eV, but tunable to low bandgap
Exciton diffusion		10-100 nm
Carrier mobility	100-10^4 $cm^2V^{-1}s^{-1}$	1 $cm^2V^{-1}s^{-1}$ for highly ordered structure, typically much lower than 10^{-3} $cm^2V^{-1}s^{-1}$
Mobility and temperature	temperature increase, mobility decrease	temperature increase, mobility increase

Above table shows some of the major differences of organic and In-organic solar cell operations. The electron hole pair are generally free carriers in inorganic where as in the organic it is tightly bound. The charge carrier generation is found in entire cell in in organic whereas at the interface in inorganic. Below table shows some of the major differences of organic and inorganic solar cell operations.

2.1.4 Dye sensitized Solar Cell

Dye sensitized Solar Cell is a type of organic solar cell which is environmental friendly, low cost. Easy fabrication and relatively has good efficiency. Figure 2.6 shows the structure of dye sensitized solar cell (DSSC) [18]. A Standard DSSC consists of a photo anode which is transparent type FTO/TCO glass which is coated with Metal oxide nanoparticles (TiO2) and then dipped in some form of dye, counter electrode is a platinum coated FTO/TCO glass and tri-iodide/iodide injected electrolyte between them.

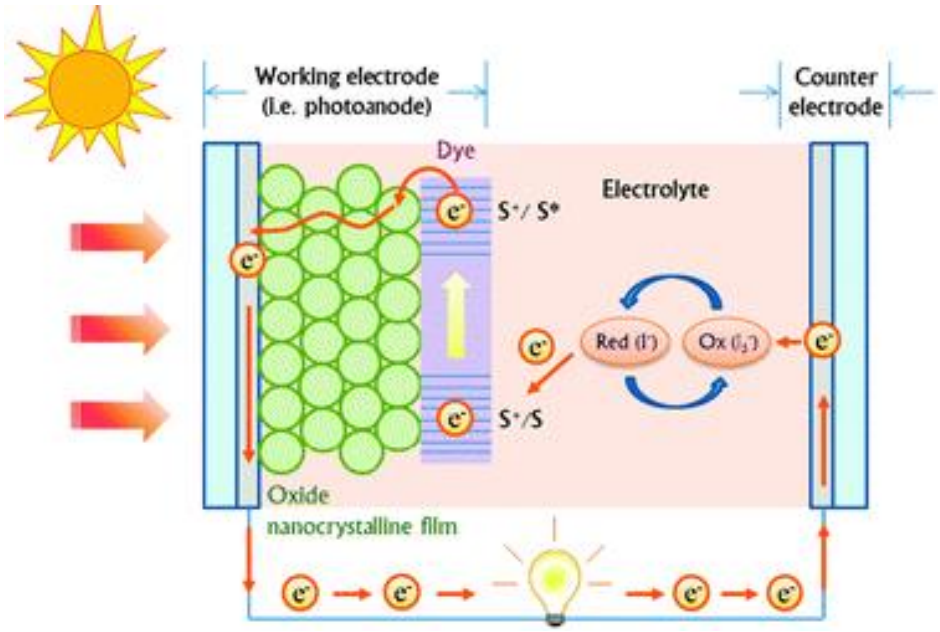

Figure 2.6 Structure of dye sensitized solar cell-– modified from [18]

Under the solar illumination, photons are absorbed by the dye which results in excitation of an electron from the ground state(S) to the excited state(S*) which is referred as highest occupied molecular orbital (HOMO) to lowest unoccupied molecular orbital (LUMO) [19].

$$TiO_2|S + h\vartheta \rightarrow TiO_2|S^* \tag{2.1}$$

Where, h is Planck's constant, ϑ is photon frequency, hϑ is photon energy. The electron in excited state is injected into the conduction band of TiO2 oxidizing the dye molecule (S+). The electrons are travelled through an external load to reach the counter electrode

$$TiO_2|S^* \rightarrow TiO_2|S^+ + e^-. \tag{2.2}$$

The reduction and oxidation process takes place at the electrolyte for electron transfer and tri-iodide is reduced to iodide

$$I_3^- + 2e^- \rightarrow 3I^-. \quad (2.3)$$

Figure 2.6. Shows the different charge transfer process in the DSSC. The recombination loss occurs during this process in which the decay of electrons occur from LUMO to HOME of the dyes as shown in figure 2.7. This process results in degrading the cell efficiency hence, an ultrafast response is required during electron injection from the dye to TiO2 for the regeneration of oxidized dye [19].

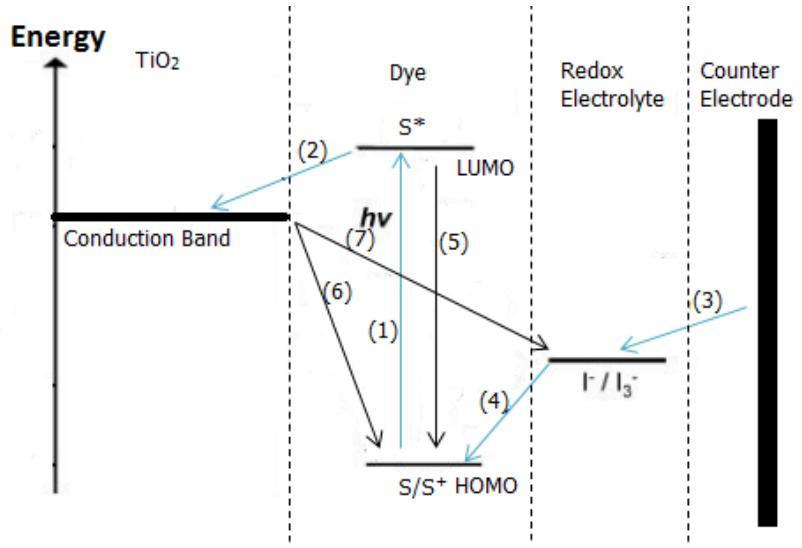

Fig 2. 7. DSSC showing different charge transfer processes. Modified from [19]

2.2 Energy Storage

Storage of energy is important for appropriate consumption of energy when required and avoid the wastage of energy. Hence this is achieved by storage of energy. Storage can be done in short term or long term. Energy storage is been widely useful from mobile energy storage to hydro storages for electricity supply. Figure 2.8 shows the types of energy storage technology which are widely used in power management and batteries are addressed to have many technology within the general shape like high energy

capacitors, high power flywheels, super capacitors and long duration flywheels. Therefore, Batteries have gained huge attention in the past for its high energy storage capacity and configurable discharge time controls for different type of power applications.

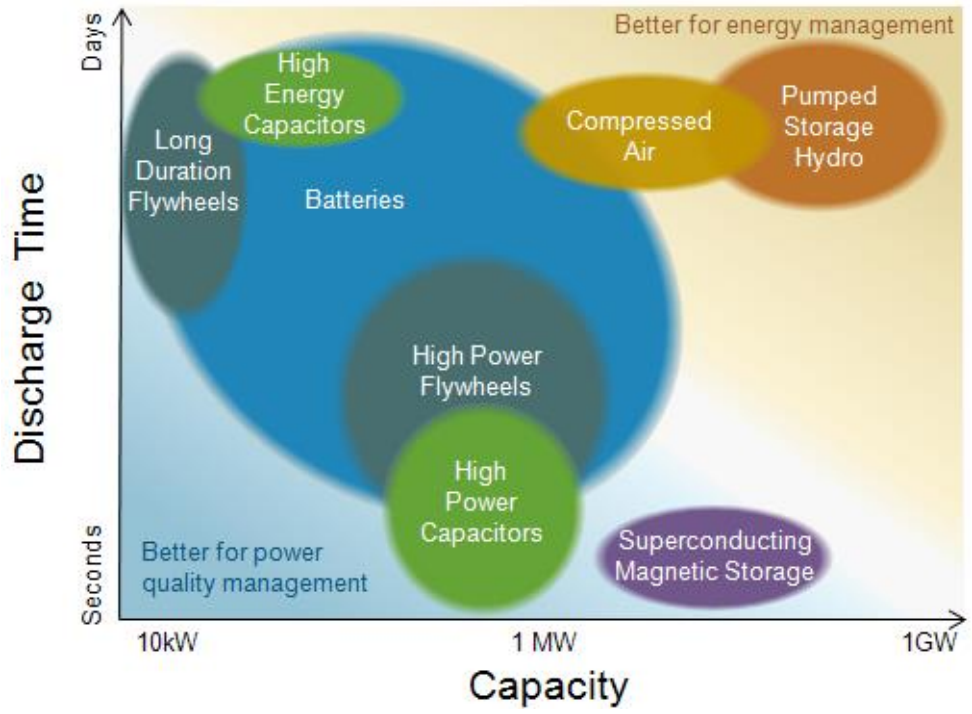

Figure 2.8. Types of energy storage for power management- modified from [20]

Table 2 shows the different battery technologies and their reported capacity, cycle life, energy efficiency with their commercial advantages and disadvantages. Lead acid batteries have relatively good cycle life but very low specific energy which make them limited for industrial applications. Also, lead is been reported has an environment hazardous material which make them less friendly for commercial usage. Nickle cadmium batteries have similar issue as that of lead-acid based batteries. Nickle metal based batteries are very expensive and low efficient which make them unattractive and Sulphur based batteries have high production cost and it operates at very high temperature of around 300^{o}C which make them very limited on usage. Lithium based battery have been a huge

attraction due to its attractive energy density, high efficient with higher operating voltage compared to other battery technologies.

Table 3: Different types of battery performance [22]

Battery	Specific Energy (Wh/kg)	Cycle Life	Energy Efficiency (%)	Nominal cell voltage (V)	Advantages	Disadvantages
Lead Acid	30-50	400-1200	75-85	2	Safe, lower cost	Low energy density, toxic, low cycle life
Nickel-Cadmium (Ni-Cd)	30-80	1000-2000	75	1.25	Long life compared to lead acid	Memory effect, toxic
Nickel-Metal Hydride (Ni-MH)	60-120	1000-2000	70	1.25	Reasonable energy density, longer life	high cost, low efficiency
Sodium Sulphur (NaS)	100	4500	89-92	2	high energy density, long life	Production cost, Operates at high temp> 300°C
Lead-Carbon	-	2500	-	-	Long life	-
Lithium-Ion ($LiCoO_2$)	150-190	500-1000	>95	3.6	High specific energy	Expensive, safety concern

Figure 2.9 shows the different battery technology performances with respect to their energy density. Lithium based batteries have gain more attention due to its high energy density of around 400 to 1700 KWH/Kg,[21] more compact designs for different mobile application, low cost and environmental friendly compared to lead acid and other sodium based batteries.

There is been continues ongoing improvements on li-ion battery to enhance its performance in terms of packaging and efficiency. As the electrolytes used are highly reactive to atmosphere and cause corrosion or even sometime explosion if it is exposed to air, therefore effective packaging is required to enhance the safety and also optimization of electrode material for low cost, high performance battery for higher energy density and

electrolyte modifications for increased life cycle and energy density of the lithium based batteries.

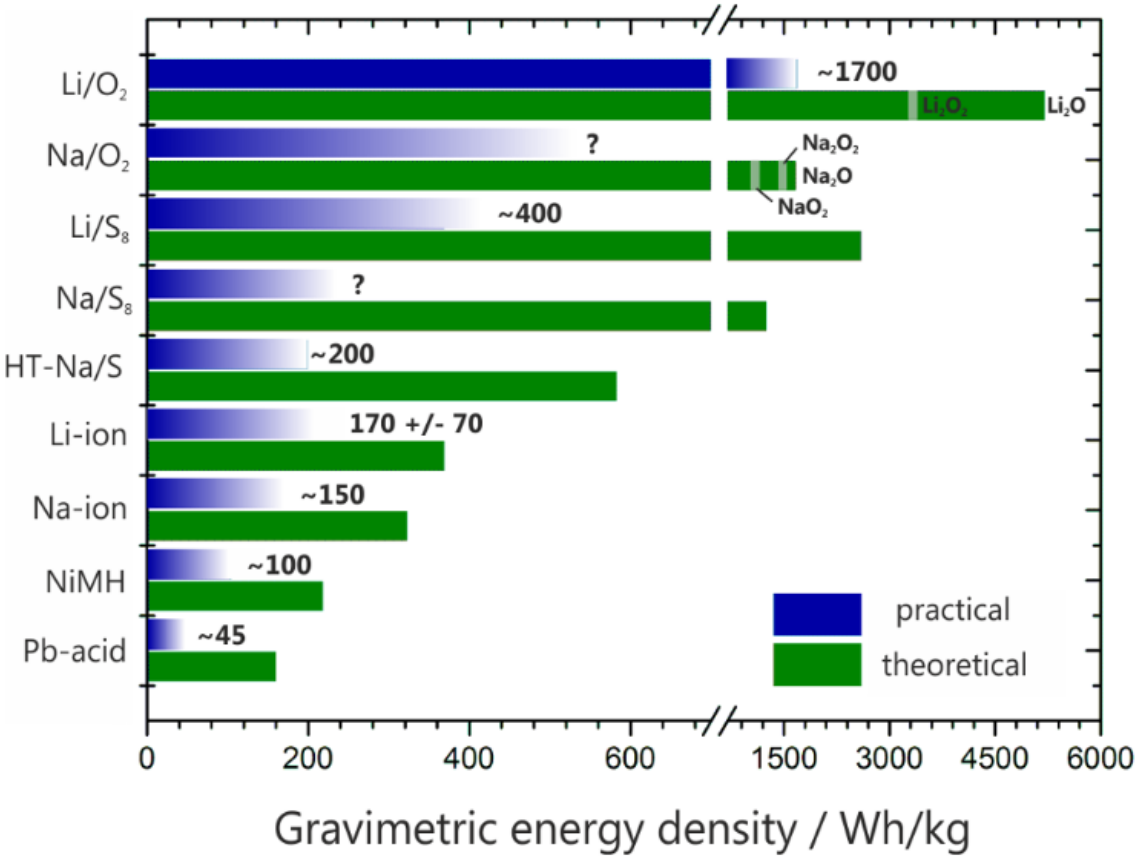

Figure 2.9 Different type of battery storage technology with their theoretical expected energy density vs. practical responses- modified from [21]

2.2.1 Lithium ion Batteries

Lithium ion batteries are electrochemical energy storage devices where chemical energy is converted into electricity [25]. It consist of an anode which uses a carbon based material coated on copper foil, cathode which uses a lithium based material coated on an aluminum foil and a polymer material called separator which separates the two electrodes physically and they are ionically connected by electrolyte on both side which are lithium

based electrolyte these type of batteries are generally called full cell as both electrodes contribute in determining the efficiency of a battery [28].

Figure 2.9 shows the schematic working of a half-cell they are useful in determining the energy density and off set voltage of a working electrode in which a particular material can behave like an anode or a cathode is a full cell. Lithium metal acts as an infinite source of Li ions which helps in understanding the electrochemical property of a working electrode for further used as a full cell [28]. The following chemical reaction shows the reduction and oxidation process taken place in a Half-cell.

$$\text{Charging: } Li_xC_6 \rightarrow C_6 + xLi$$
$$\text{Discharging: } C_6 + xLi \rightarrow Li_xC_6 \qquad (2.19)$$

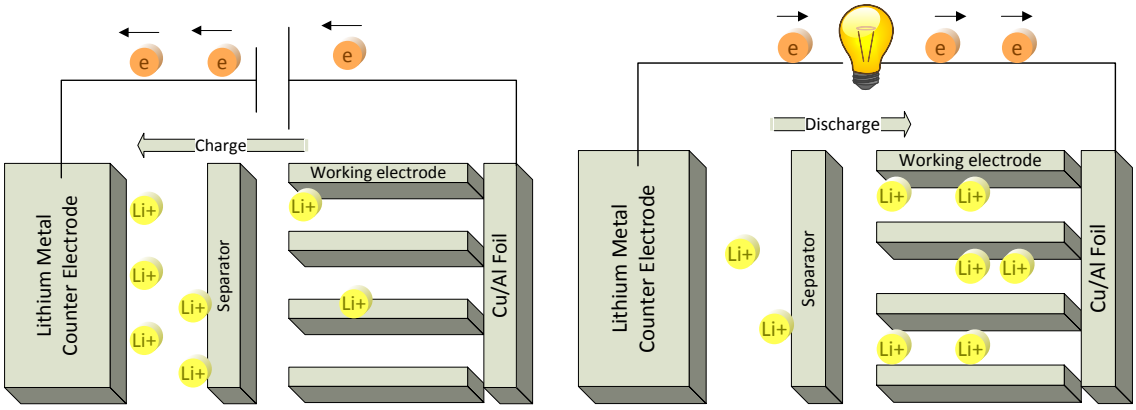

Figure 2.10. Schematic of Half-cell Charge and Discharge mechanism

Figure 2.10 and figure 2.11 shows charge and discharge mechanism of lithium ion battery. Graphite is well known for high efficient carbon material and lithium cobalt oxide (LiCoO2) as cathode material and porous polyethylene as a separator which physically separates the two electrodes and lithium salt (LiPF6) as electrolyte.

When the External potential pulls electrons out of the cathode towards the anode. Lithium ions (Li+) moves from cathode to anode via electrolyte and lithium ions are deposited onto the graphite layers and oxidation process takes place. Hence, the lithium charges being collected [28].

Charging reaction: $C_6 + xLi^+ + xe^- \rightarrow Li_xC_6$

$LiCoO_2 \rightarrow Li_{1-x}CoO_2 + xLi^+ + xe^-$

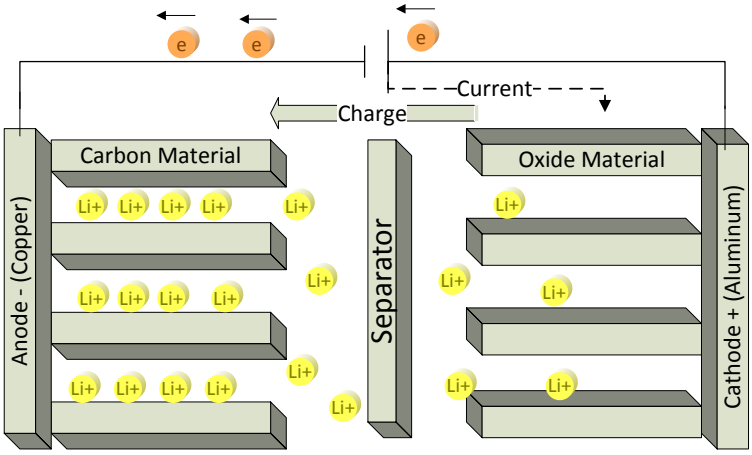

Figure 2.11. Charging mechanism of a full cell lithium ion battery

During the battery discharge, Li^+ ions move back from anode to cathode via electrolyte and electrons flow through the external circuit through a load as shown in the figure 2.10 and reduction process takes place discharging the lithium ions from anode.

Discharge reaction: $Li_xC_6 \rightarrow C_6 + xLi^+ + xe^-$

$Li_{1-x}CoO_2 + xLi^+ + xe^- \rightarrow LiCoO_2$

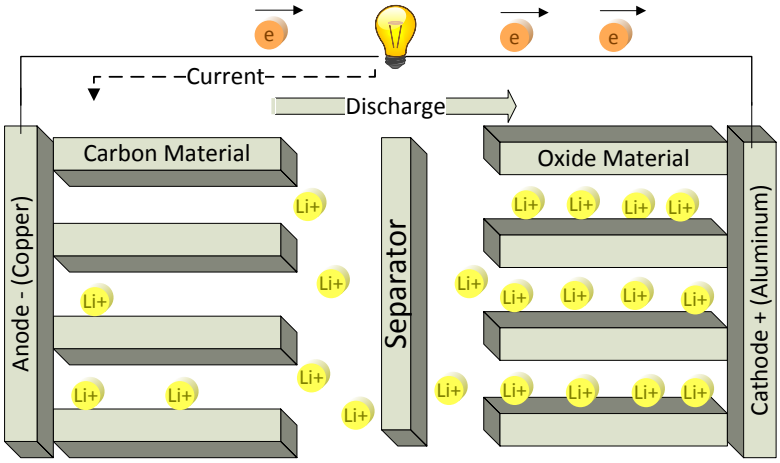

Figure 2.12. Discharge mechanism of a full cell lithium ion battery

2.2.2 Solar cell (DSSC) integrated with Lithium ion battery

The dye sensitized solar cell-Lithium ion battery integrated device consists of solar cell on top and Li-ion battery on bottom with a common titanium substrate in between as shown in Figure 2.13 For photo conversion of this integrated structure, DSSC requires rear-illumination which means the sunlight has to be incident from the counter electrode side. Upon solar rear-illumination, the photo generated electrons will be injected to conduction band of TiO2 from dye and transported along Ti foil to the anode of Li-ion battery (TiO2). This causes charging of Li-on battery. The reaction at the cathode releases lithium ions towards anode of Li-ion battery and electrons towards counter electrode of DSSC via external wire [29] as

$$LiCoO_2 \rightarrow Li_{1-x}CoO_2 + xLi^+ + xe^-. \qquad (2.22)$$

The lithium ion travel via electrolyte into the anode of Li-ion battery. The photo-generated electrons that reach the anode react with these Li-ions to induce the following reaction [28].

$$TiO_2 + xLi^+ + xe^- \rightarrow Li_xTiO_2. \quad (2.23)$$

Discharging occurs via a load connected across the li-ion battery under no solar illumination. During discharging, the same process takes place as in the case of a typical stand-alone li-ion battery.

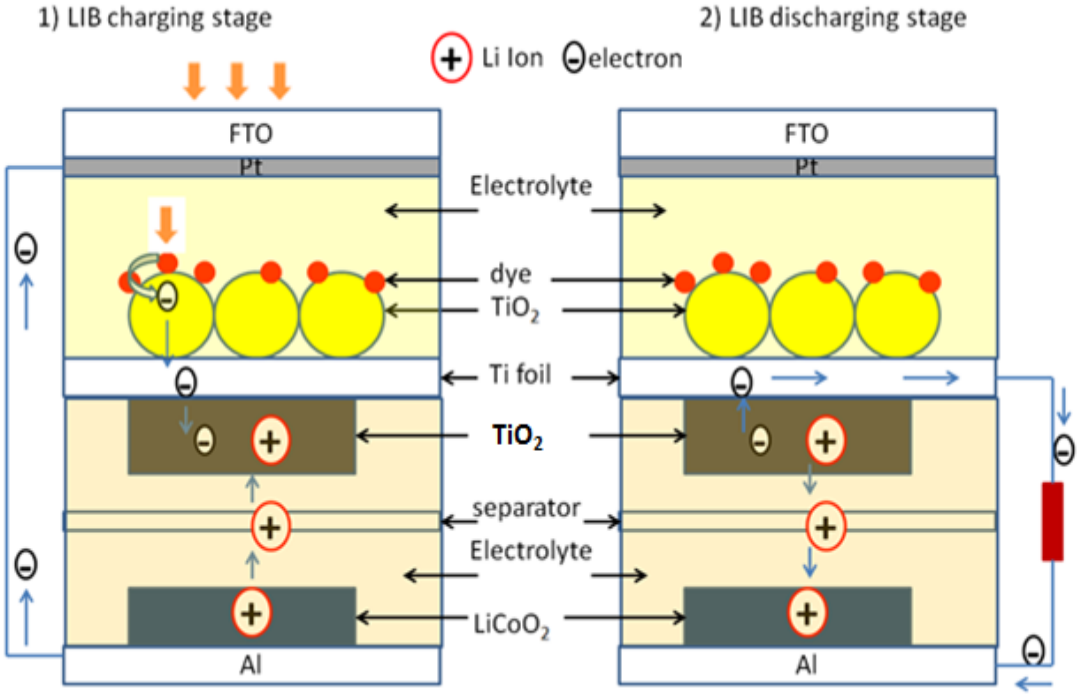

Figure 2.13 Schematic showing working of an integrated structure of dye sensitized solar cell and Li-ion battery

The performance of such an integrated device is affected by several factors. The output is the discharge energy of the Li-ion battery and input is the incident light energy. A parameter called entire energy conversion and storage efficiency (η_{entire}) is used to quantify the performance of such integrated device [29] as

$$\eta_{entire} = \int VIdt/P_{in}t_1\eta_{sc} \quad (2.24)$$

where, V is the instantaneous discharge voltage, dt is the time interval, I is the discharge current, Pin is the incident light power density, t1 is the illumination time during photo charging, ηsc is the efficiency of solar cell. The integration of the discharge voltage and current with respect to time gives the total output energy of the integrated device.

Chapter 3 : Experimental Procedure

3.1 Fabrication of Commercial coin cell Lithium-ion battery

3.1.1 Full cell Battery

Figure 3.1. Shows the fabrication procedure of coin cell lithium ion battery. Commercially available graphite coated on copper (cu) foil wafers were used as anode and lithium cobalt oxide ($LiCoO_2$) coated on aluminum foil wafers were used as cathode and lithium hexafluorophosphate [1 M LiPF6 dissolved in EC/DMC/DEC (1:1:1 by volume ratio)] is used as liquid electrolyte to ionically conduct and polyvinylidene fluoride (PVDF) polymer is used as a separator to physically separate the two electrodes.

All fabrication procedure was made in glove box in argon environment as lithium is highly reactive to atmosphere. Anode was placed on stainless steel based positive case and electrolyte soaked polymer separator was placed with placing cathode on the polymer. Steel disc and spring were placed to ensure all the electrode to be in place while sealing. CR2032 die and hydraulic hand press were used to seal the two cases together and LAND CT2001A battery tester was used to characterize the electrochemical behavior of fabricated coin cell.

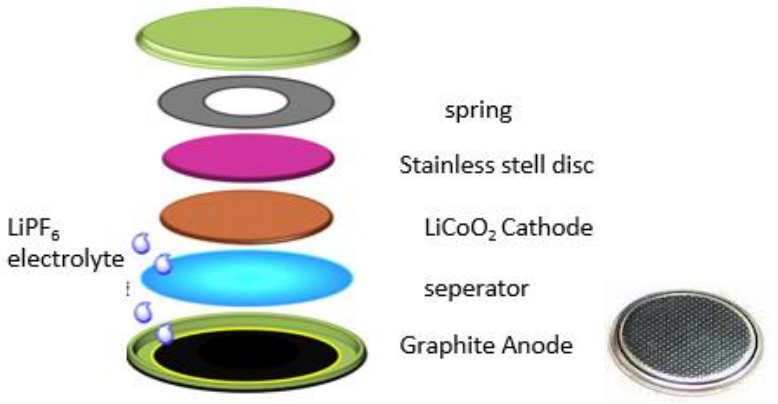

Figure 3.1. Fabrication procedure of coin cell battery-modified from [22]

Table 4 shows the electrochemical measurement parameters that are set to measure charge and discharge performance of graphite anode and lithium cobalt oxide cathode based full cell battery with a constant charge and discharge current density of 0.2mA with open circuit voltage of 3V.

Table 4 Measurement parameters of full cell battery

S.N.	Mode	Current or Voltage	Ending condition
1	Charging : constant current	0.2 mA	Cut off voltage: 4.2 V
2	Charging: constant voltage	4.2 V	Cut off current: 0.05 mA
3	Discharging : constant current	0.2 mA	Cut off voltage: 3 V

3.1.2 Half-cell battery

Figure 3.2 shows the fabrication procedure of half-cell battery. Assembly process follows similar steps of full cell battery as described in 3.1 but instead of using two electrode material, lithium metal is placed and only one working electrode is used to determine the performance of electrode.

Figure 3.2. Fabrication procedure of half-cell coin cell battery-modified from [22]

Table 5 shows the electrochemical measurement parameters that are set to measure charge and discharge performance of graphite anode based half-cell battery with a constant charge and discharge current density of 0.2mA with open circuit voltage of 3V and cut-off voltage of 0.01V to observe electrochemical behavior of the electrode.

Table 5 Measurement parameters of Half-cell battery

S.N.	Mode	Current or Voltage	Ending condition
1	Discharging : constant current	0.2 mA	Cut off voltage: 0.01 V
2	charging : constant current	0.2 mA	Cut off voltage: 3 V

3.1.3 Characterization using LAND CT2001A battery tester

In order to measure the electrochemical parameters and charge-discharge capacity of the fabricated lithium ion battery CT2001A battery tester was used as shown in the tester setup shown below. Computer interface was used in order to record cycle life of the batter which can be used for further analysis. Multiple batteries were fabricated using commercial

stainless steel case and titanium foil based thin film battery for analysis of material performance of the Lithium based battery.

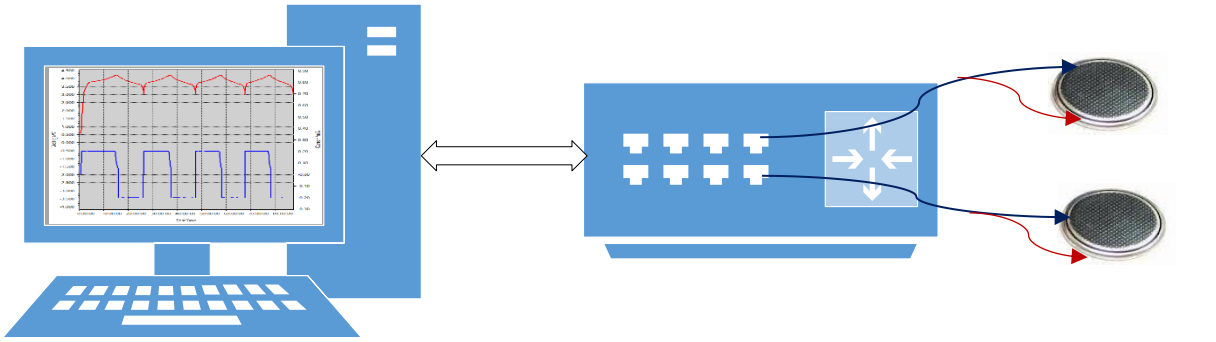

Figure 3.3. LAND CT2001A battery tester Setup

Table 6 shows the LAND CT2001A battery tester parameters for input cutoff current and voltage variations for understanding energy density and voltage capacity of battery fabrication.

Table 6 LAND CT2001A battery tester setup parameters

Mode	Current or Voltage	Ending condition
Charging : constant current	8 mA	Cut off voltage: 4.2 V
Charging: constant voltage	4.2 V	Cut off current: 0.8 mA
Discharging : constant current	8 mA	Cut off voltage: 3 V

3.2 Anatase TiO2 as an anode material for battery

Titanium dioxide or titania (TiO2, provided by aeroxide Co. Degussa with an average diameter: P25 60-70 nm) is an inorganic material which has higher voltage relative to lithium and it is very safe to use as its not highly reactive to air and it is environmental

friendly. Furthermore, most polymorphs of TiO2 (Anatase, rutile and TiO2 (B)) are incredibly stable under long cycling, even at high rates. It has a very little volume expansion within the crystalline lattice upon lithium insertion/disinsertion.

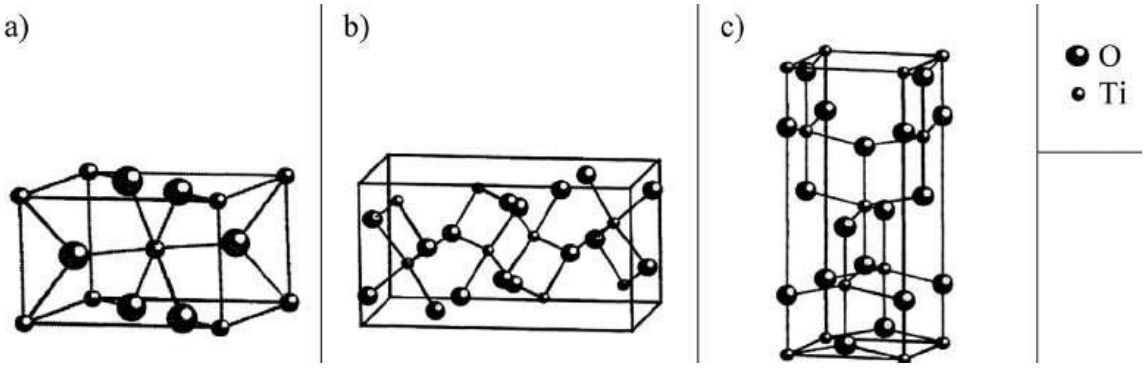

Figure 3.4 shows the resonance forms of different TiO2 materials ((a) rutile, (b) TiO2 (B) and (c) Anatase)

Table below shows the general physical property of a TiO2 material for better understanding on material selection for device fabrication.

Table 7: Physical properties of TiO2 Material

Molar mass	79.866 $g.mol^{-1}$
Appearance	White solid
Density	4.23 $g.cm^{-3}$
Melting point	1,843 °C - 3,349 °F- 2,116 K
Boiling point	2,972 °C - 5,382 °F - 3,245 K
Solubility in water	Non-soluble

3.2.1 Preparation of TiO2 based anode films

3.2.1.1 Titanium dioxide based slurry

Slurry was prepared using PVDF binder of 6wt. % dissolved in N-methl-2-pyrrolidone (NMP) solvent in order to provide adhesion while making wafers. 80wt. % active material titanium dioxide (TiO2) was mixed with 10wt. % super P carbon black as conductive additive to improve the conductivity and charge density of the material followed by mixing with the dissolved PVDF/NMP such that PVDF-NMP constitutes 10wt. % Suitable quantity of NMP was further added into the slurry for balanced viscosity. The slurry was then magnetically stirred overnight to form a uniform paste.

3.2.1.2 Titanium dioxide based anode film

Figure 3.3 shows the anode film made on copper foil using the TiO2 slurry. A copper (Cu) metal foil was spread on to a glass plate. Acetone was used to ensure there were no air bubbles between the foil and the glass plate. Using two layers of masking tape, the region to be coated was defined. The slurry was doctor bladed on to the Cu foil. The coating was dried in vacuum at 90-120 °C for ~ 12 h. The dried coated metal foil was punched into discs of 12.7 mm diameter and weighed.

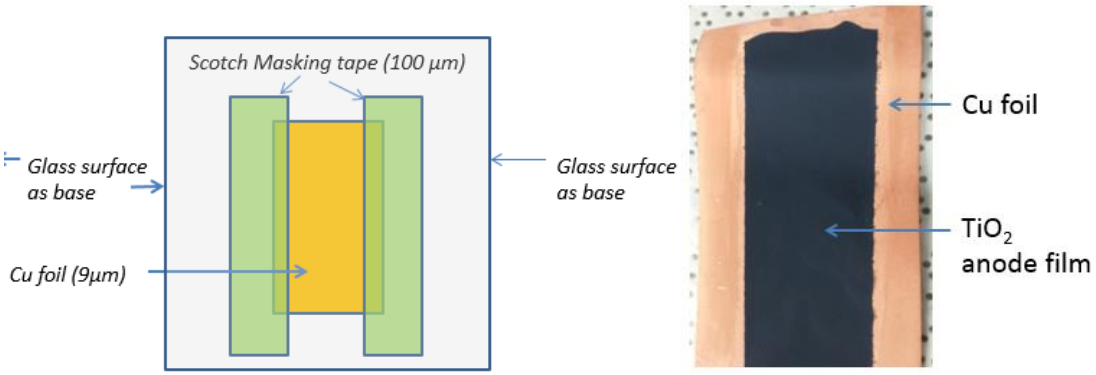

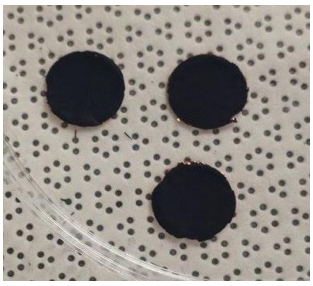

Figure 3.5 (a) Preparation of TiO_2 anode Film on Cu foil (b) After Dr. blading image (c) Foils prepared for coin cell fabrication

3.2.2 Titanium dioxide (TiO2) anode based half-cell and full cell coin cell Battery

Similar procedure of a standard half-cell and full cell fabrication procedure was followed and cell was prepared in a glove box with argon gas environment and cells were later tested using LAND CT2001A battery tester.

Figure 3.6 Fabrication procedure of TiO2 based (a) Full cell and (b) half-cell coin cell battery

Table 8 shows the electrochemical measurement parameters that are set to measure charge and discharge performance of TiO2 anode based half-cell battery with a constant charge and discharge current density of 0.08mA with open circuit voltage of 3V and cut-off voltage of 1V to observe electrochemical behavior of the electrode.

Table 8 Measurement parameters of Half-cell battery

S.N.	Mode	Current or Voltage	Ending condition
1	Discharging : constant current	0.08 mA	Cut off voltage: 1 V
2	charging : constant current	0.08 mA	Cut off voltage: 3 V

Table 9 Measurement parameters of Full cell battery

S.N.	Mode	Current or Voltage	Ending condition
1	Charging : constant current	0.08 mA	Cut off voltage: 3 V
2	Discharging : constant current	0.08 mA	Cut off voltage: 1 V

3.2.3 Titanium dioxide (TiO2) anode based thin film Li-ion battery on Titanium substrate

Titanium foil was used as a substrate for thin film fabrication. Ti foil was cleaned using detergent, followed with ultra-sonication for 30 mins in acetone and cleaning in isopropyl alcohol. TiO2 slurry was then prepared by using the standard procedure as mention in 3.3.1. The slurry was then coated on Ti substrate using circular mask tape as shown in figure 3.5. And was dried in vacuum heater in 100 °C for 12 hours. The desired thickness of ~50-60 µm, was achieved by repeating the coating procedure twice. The sample was then transferred in the Argon filled glove box. Polymer polyethylene separator was soaked into $LiPF_6$ electrolyte and was placed on anode. Commercial LiCoO2 on aluminum foil cathode was placed on rinsed separator and the cell was sealed using acid resistant epoxy and was waited for 8 hours on epoxy curing. Finally the cell was characterized using LAND CT2001A battery tester with a voltage range of 1-3V.

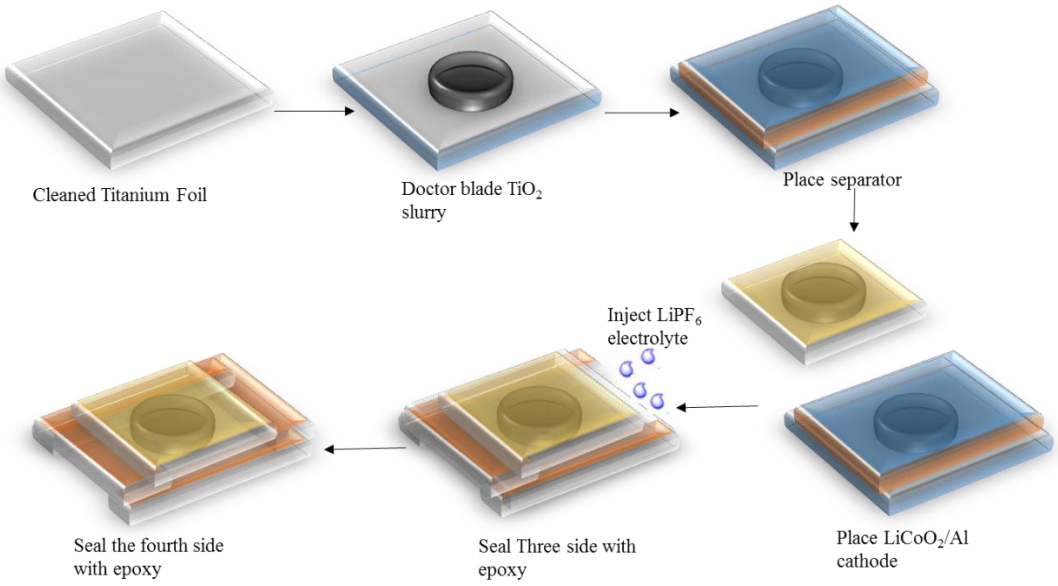

Figure 3.7 Fabrication of thin film Li-ion battery

3.3 Using dc power supply as charging source

As a single solar cell do not have an ability to supply enough voltage required to charge a battery, a series of solar cell can be used, but this leads to design complication in fabricating a tandem DSSC structure or multiple solar cell to connect in series which consumes huge space for the voltage and current requirements to charge lithium ion battery. Hence a programmable DC supply of 0.6V and a current limit of 1mA is being used (P_{in}, max = 0.6 mW) was applied to the boost convertor bq25504EVM and LabVIEW was programmed for input voltage and current controller circuit for testing the battery charging. Figure 3.7. Shows the lab setup for charging the battery with boost convertor with the help of using a DC power supply.

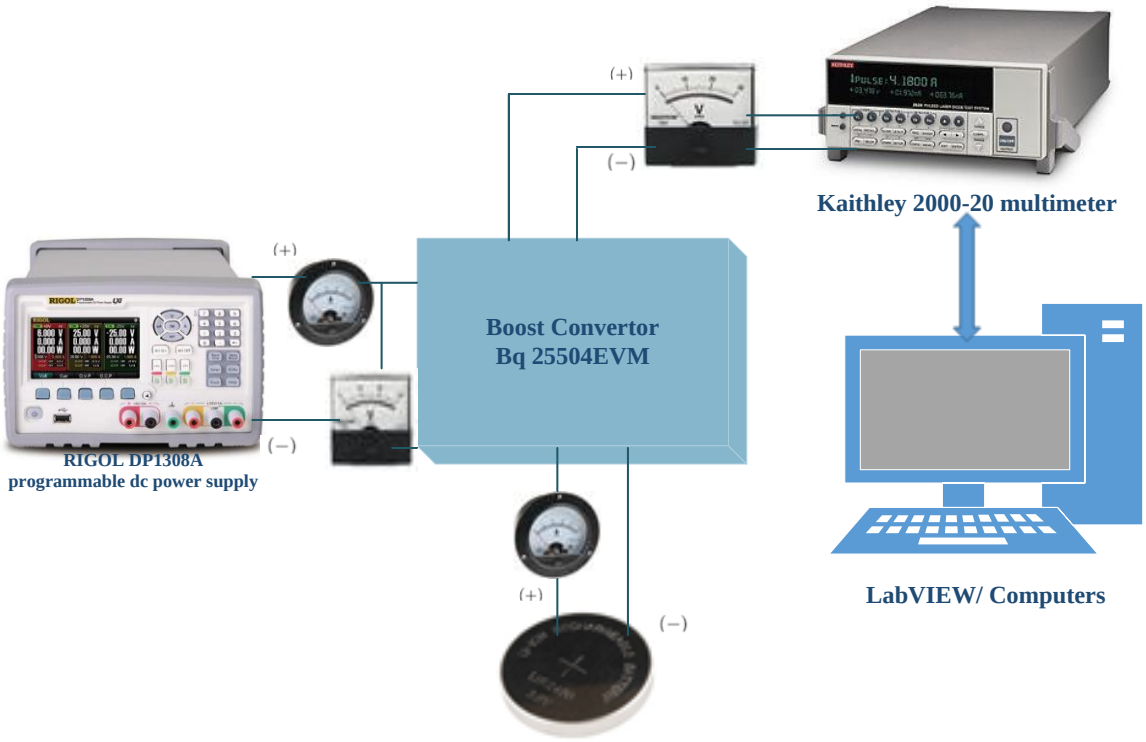

Figure 3. 8 Schematic for battery charging using dc power supply and boost converter

3.4 Dye sensitized solar cell (DSSC)

3.4.1 Fabrication procedure

Figure 3.6 shows the standard fabrication procedure of Dye sensitized solar cell (DSSC). Florine doped Tin Oxide (FTO) glass was used as substrate for photo anode and counter electrode. FTO was cleaned using detergent and deionized water and ultra-sonicated for 30 mins followed by acetone and IPA cleaning. TiO2 compact layer was deposited by spin coating at 3000 rpm for 20 seconds substrate using a 0.025 Mtitanium di-isopropoxide bis (acetylacetonate) solution in anhydrous ethanol, and was sintered at 475 °C for 30 minutes and the process was repeated to achieve desired thickness of compact layer. TiO_2 mesoporous layer was made by doctor blading nanocrystalline TiO2 layer (Ti-

nanoxide HT/SP, solaronix) using a circular opening mask with area of 0.125 cm2 was made using a scotch tape and was peeled off after doctor blade. Then the mesoporous layer was sintered at 125°C for 15 minutes and 475 °C for 30 min in order to achieve the uniform adhesion of the layer. The process was repeated to achieve ~12-14 microns thickness.

A light scattering layer was deposited using TiO_2 (Ti-Nanoxide R/SP, Solaronix) on to the mesoporous layer by similar process of doctor blading and was sintered at 475 °C for 30 min to achieve ~4-5 microns thickness. The film was then dipped into 40mM of aqueous solution of titanium tetrachloride ($TiCl_4$) at 70 °C for 30 min and was rinsed with de-ionized water and anhydrous ethanol, to remove excess $TiCl_4$ solution from the surface and the film was sintered at 125°C for 15 minutes and 475 °C for 30 min. The temperature was later dropped to 80 °C for soaking the film into 0.3 mM N-719 (Solaronix Ruthenizer 535-bisTBA) dye solution in anhydrous acetonitrile and anhydrous tert-butanol (1:1 by volume) for 24 hours. Finally, the photo anode was kept in acetonitrile solution for 3 hours to remove any dye molecules not anchored to the TiO_2 layer.

FTO glass was cleaned in the above mentioned cleaning process for counter electrode. Platinum deposition using 20mM platinum (Pt) solution was spin coated and in 3000 rpm for 20 seconds and was sintered at 400 °C for 15 minutes and the process was repeated to get desired thickness of ~10-12 microns. The surlyn sealing mask was used to sandwich photo anode and counter electrode together and electrolyte was injected using pipette and the cell was sealed using a hot glue and characterization was performed using a solar simulator.

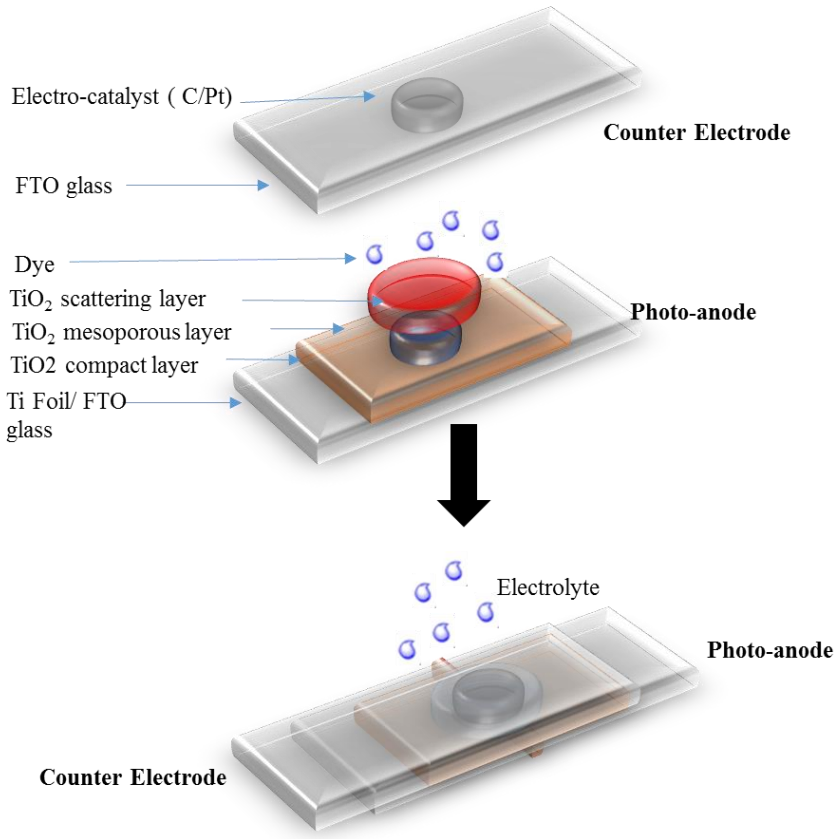

Figure 3.9 Fabrication procedure of standard Dye sensitized solar cell

3.4.2 Characterization setup of DSSC solar cell

The fabricated DSSC was charged using a xenon halogen arc lamp with AM 1.5 filter was used as a light source which was in the form of a solar simulator which was turned on for 30 minutes for uniform illumination of photons. Bias voltage was applied for current measurement and Agilent 4155C semiconductor (S.C) parameter analyzer unit which was controlled form PC using desktop easy-expert software and the source/measuring unit 3 (SMU3) device was programmed in voltage sweep mode of 0V to 1V in steps of 10mV to measure the short circuit at different voltages and source/measuring unit 4 (SMU4) was programmed as constant voltage mode. National renewable energy

laboratory (NREL) calibrated Hamamatsu S1133 photo detector was used to calibrate the distance (light intensity of 1000 W/m^2) between solar simulator and the photodetector until the measured short circuit current matches the NREL data. The photodetector was removed after calibration for testing the solar cell. The current was recorded at each bias voltage and current density versus voltage (J-V) characterization was plotted using computer when the device was under test and the characterization was used to determined short circuit current (J_{sc}), Open circuit voltage (V_{oc}), Fill Factor and efficiency. To determine the performance of solar cell performance.

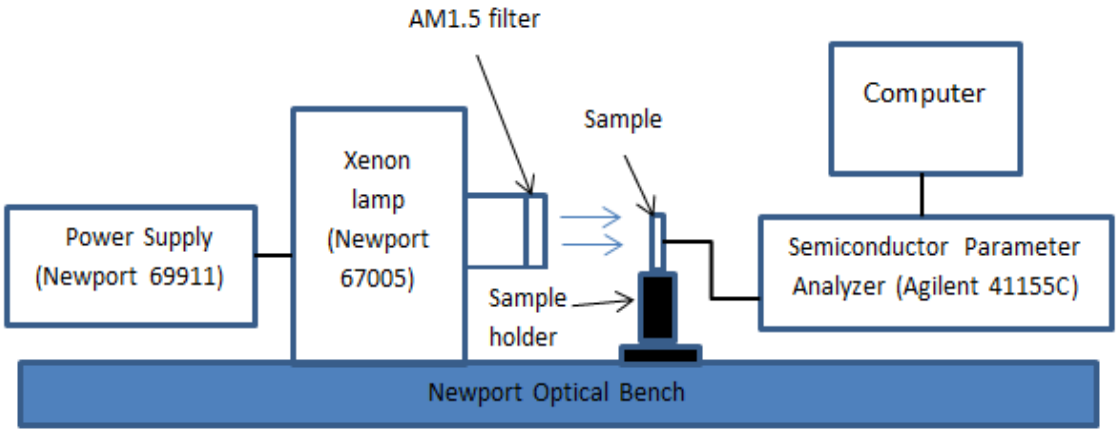

Figure 3.10 Schematic setup of DSSC characterization

3.5 Integrated device

3.5.1 Fabrication of Integrated DSSC-Li-ion Battery

Figure 3.7 shows the fabrication procedure of integrated DSSC with battery using a common titanium foil substrate. Titanium foil was diced into desired size and was cleaned using detergent and deionized water and ultra-sonicated for 30 mins followed by acetone and IPA cleaning. Double TiO2 compact layer was deposited by spin coating and sintering at 475 °C for 30 mins. Double TiO2 main layer was doctor bladed and sintered at 475 °C

for 30 mins. Doctor blade TiO2 scattering layer and oven sinter at 475 °C for 30 mins and 40 mM TiCl4 heat treatment @ 70 °C of the anode and oven sinter at 475 °C for 30 mins and Dye absorption using 0.3 mM N719 dye for 18 h-24h and similar procedure of counter electrode was carried out using the standard DSSC fabrication procedure.

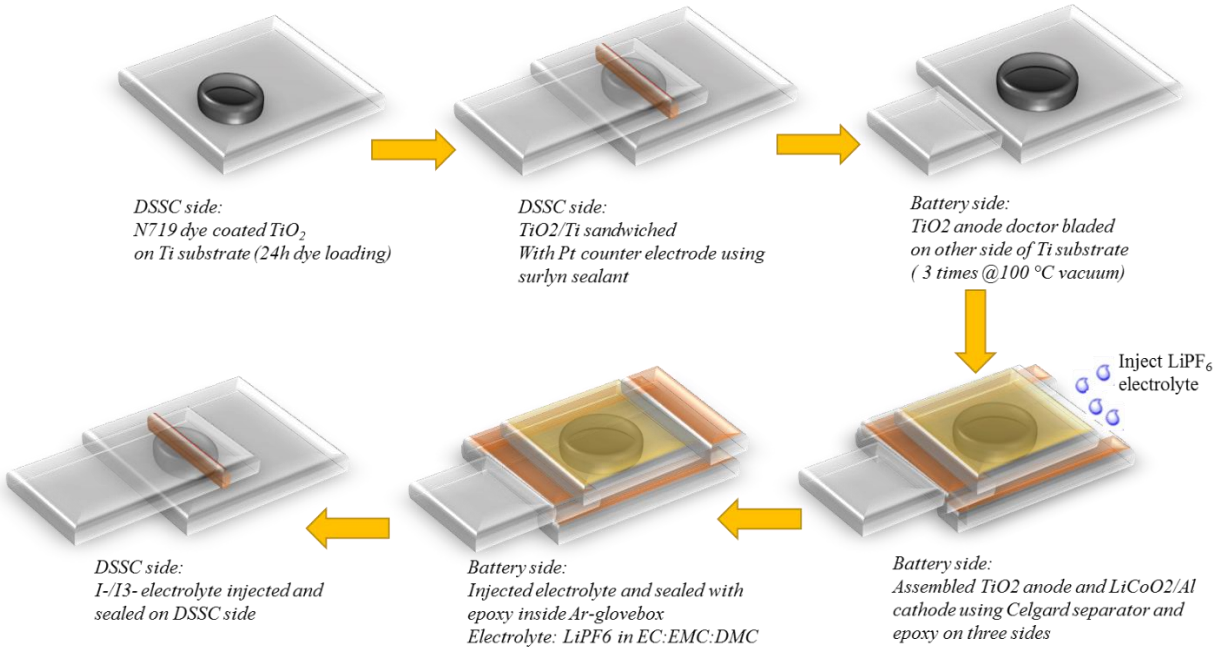

Figure 3.11 Fabrication of integrated Battery and DSSC using Titanium foil as common substrate

Figure 3.8. Shows the battery side and DSSC side of the integrated device using the common titanium foil electrode as anode and aluminum foil cathode at the battery side and FTO cathode on the DSSC side for thin film storage for mobile application.

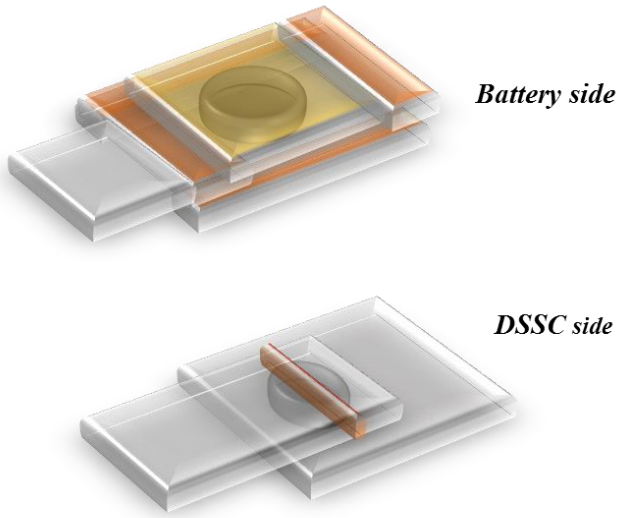

Figure 3.12 Schematic of battery and DSSC side integrated device

3.5.2 Characterization of charge/discharge setup of battery and commercial solar panel

Figure 3.9 (a) shows the charging of lithium ion battery using a commercial thin film solar Copper Indium Diselenide (CIS) solar panel which had a maximum power output of 0.25 W with 80 mA @ 3.2 Vdc which are connected in series to provide higher voltage and was charged using solar simulator of xenon arc lamp with AM 1.5 of 500 W placed around 45°. The solar cell was kept 7X7 inch from the lamp. Diode was used to prevent reverse current flow from battery to the solar panel the battery was discharged using a resistor as load of 150 Ω for 0.5 C discharge.

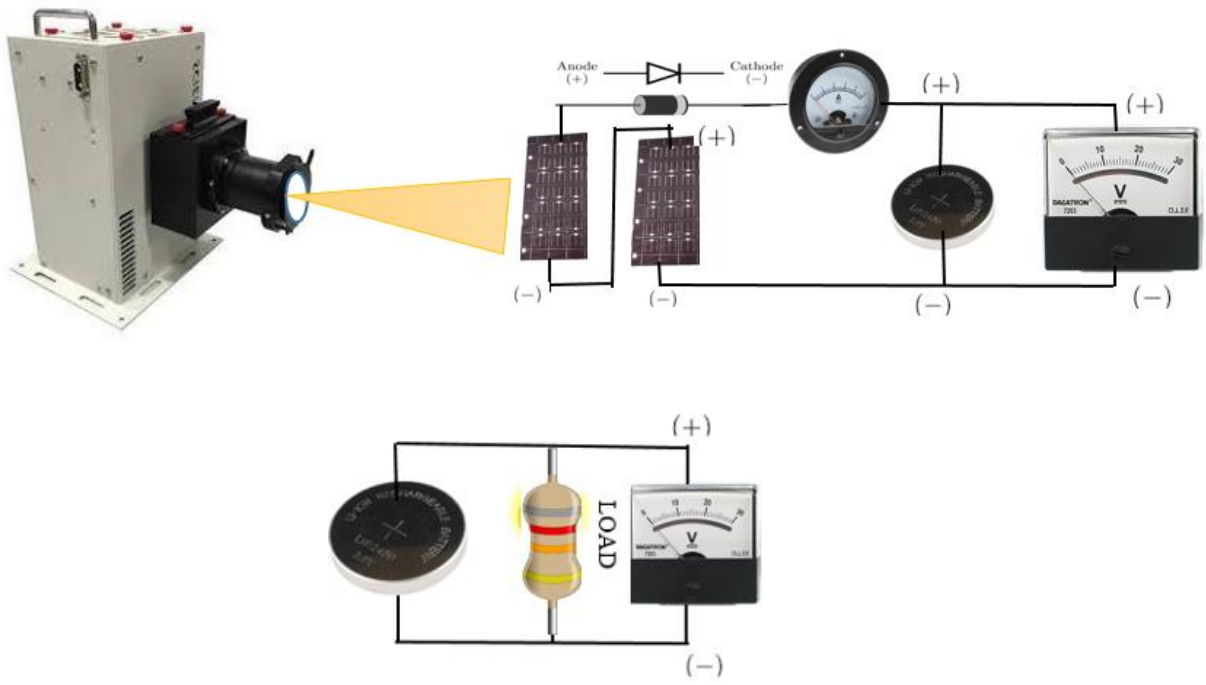

Figure 3.13 Schematic setup of charge/discharge of commercial lithium ion battery using standard DSSC with solar simulator (a) Charge setup (b) Discharge setup

3.5.3 Charge-discharge Characterization setup of a standard DSSC and coin cell based battery using boost converter

Figure shows the characterization setup of fabricated DSSC and TiO_2 anode based coin cell battery. Xenon arc lamp was used as a solar simulator with AM 1.5 illumination of 100 $mWcm^{-2}$ and was illuminated at the front side of the DSSC solar cell, as the photo anode was the transparent side of the solar cell and the input voltage and current was recorded . Boost convertor Bq25504EMV was used to charge the battery and the charging cycling of the battery was recording using the Labview program once every minute and the battery current and voltage was recorded using the multimeter [30]. The 3V fully charged battery was discharge to 1v using the LAND CT2001A battery tester and the discharge

cycle was plotted. The charge/discharge storage efficiency was calculated after several cycle of battery performance.

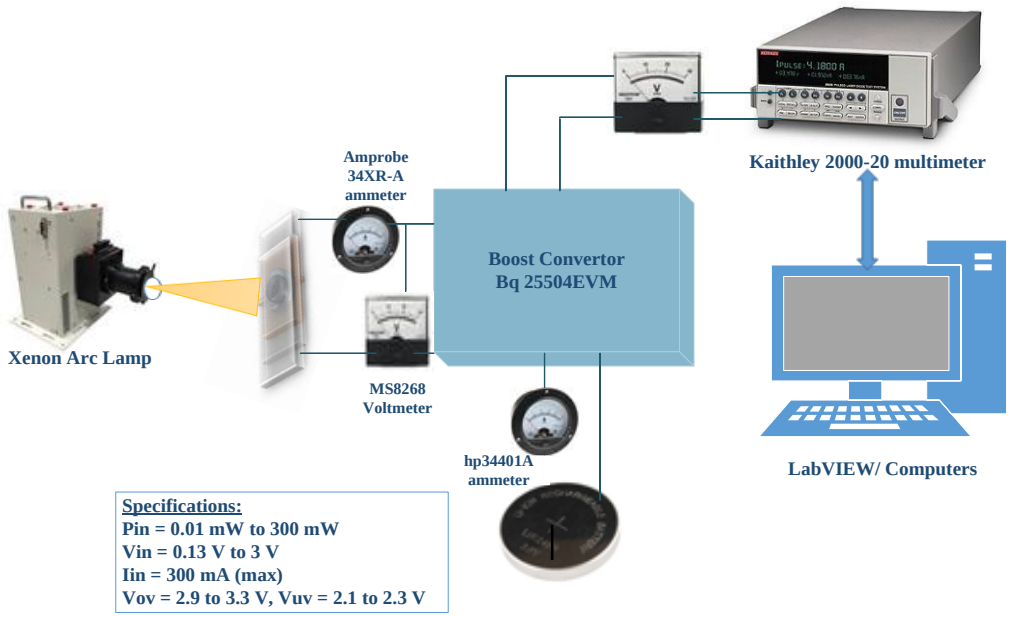

Figure 3.14 Characterization setup of TiO2 coin cell battery using DSSC solar cell with the help of Boost convertor

3.5.4 Characterization of Integrated DSSC-Li-ion Battery

Xenon arc lamp of AM 1.5 illumination with 100 $mWcm^{-2}$ was used as light source for DSSC, the light was illuminated from the rear side of the solar cell through counter electrode as it was the transparent side of the solar cell . Boost convertor was used as a voltage multiplier for large input voltage and current to charge the thin film Li-ion Battery. Titanium (Ti) foil was used as a common electrode for charge transport layer between DSSC and battery. The charging cycling of the battery was recording using the Labview program once every minute and the battery current and voltage was recorded using the multimeter. The 3V fully charged battery was discharge to 1v using the LAND CT2001A

battery tester and the discharge cycle was plotted. The charge/discharge storage efficiency was calculated after several cycle of battery performance.

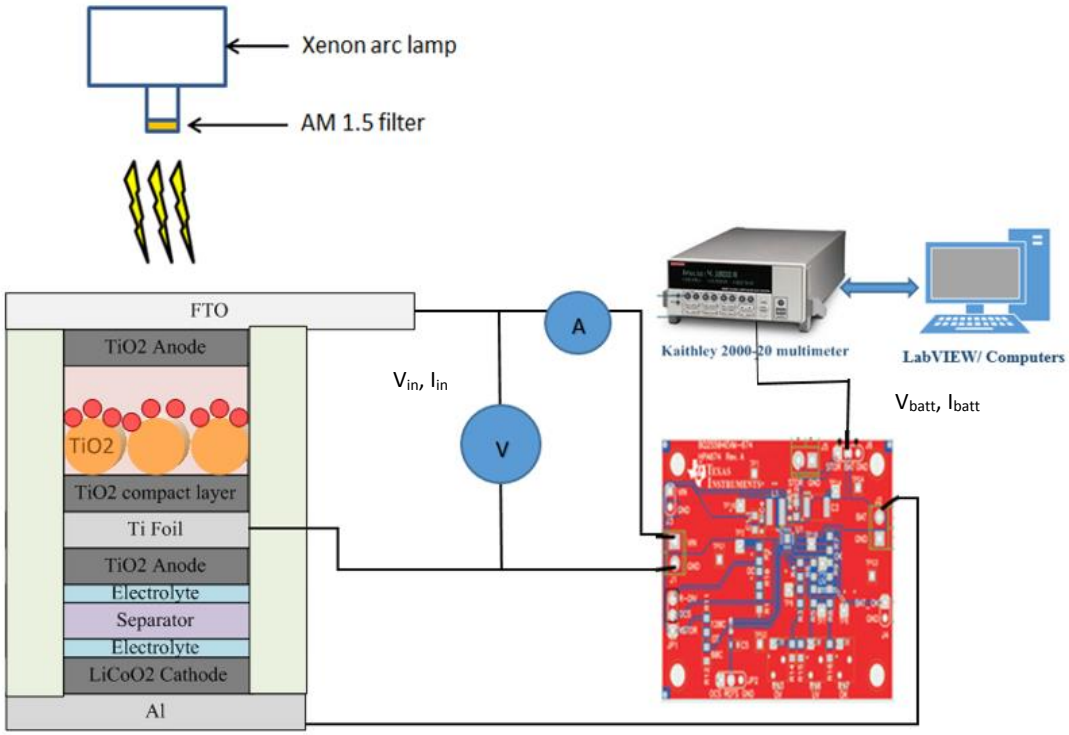

Figure 3.15 Characterization setup of Integrated DSSC-Li-ion Battery (a) Charging

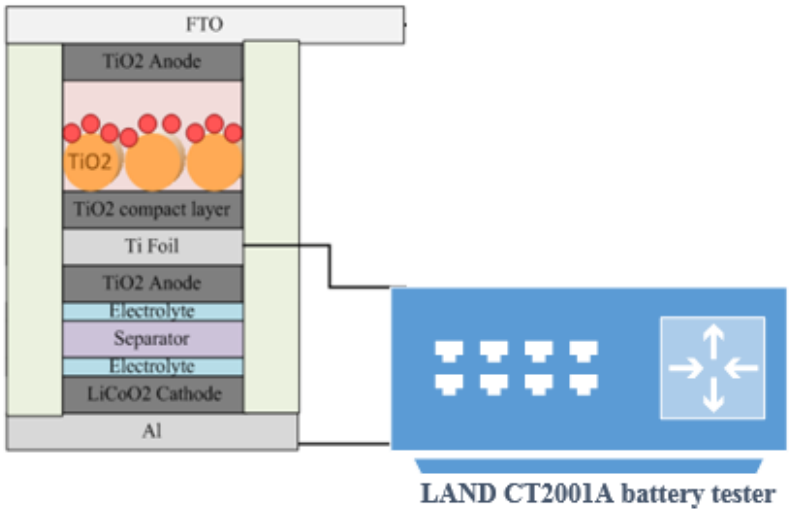

(b) Discharging characterization

Following equations are used to calculate the Energy conversion and storage parameters for integrated device:

- Efficiency of solar cell,

$$\eta_1 = (J_{sc} \times V_{oc} \times FF)/P_{in} \times 100\ \%$$

where, J_{sc} = short-circuit current ($mAcm^{-2}$)
V_{oc} = open-circuit voltage (V)
FF = Fill factor
P_{in}= incident light power density (100 $mWcm^{-2}$)

- Total efficiency of integrated device,

$$\eta_2 = {E_{discharge}}/{(P_{in} \times A \times t)} \times 100\%$$

where, $E_{discharge}$ = discharge energy (mWh)
A = effective area of solar cell (cm^2)
t = photo-charge time (h)

- Storage efficiency

$$\eta_3 = {\eta_2}/{(\eta_1 \times \eta_{converter})} \times 100\%$$

Chapter 4 : Result and analysis

4.1 Charge-discharge characteristics of commercial lithium ion coin cell battery

4.1.1 Full cell lithium ion battery

Figure 4.1 shows the charge-discharge cycle of a standard 40mAH rated coin cell lithium ion full cell battery with a graphite anode and LiCoO2 cathode which is a standard commercial lithium ion battery and was characterized using land CT2001A Battery tester at the higher input current rate of 8mA. The battery was initially fully charged with ~9.749 mAh to charge 4.2V and was discharged at 31.697 mAh. The battery was charged and discharged for multiple cycles and was recorded and an average overall charge-discharge efficiency of ~80% was achieved.

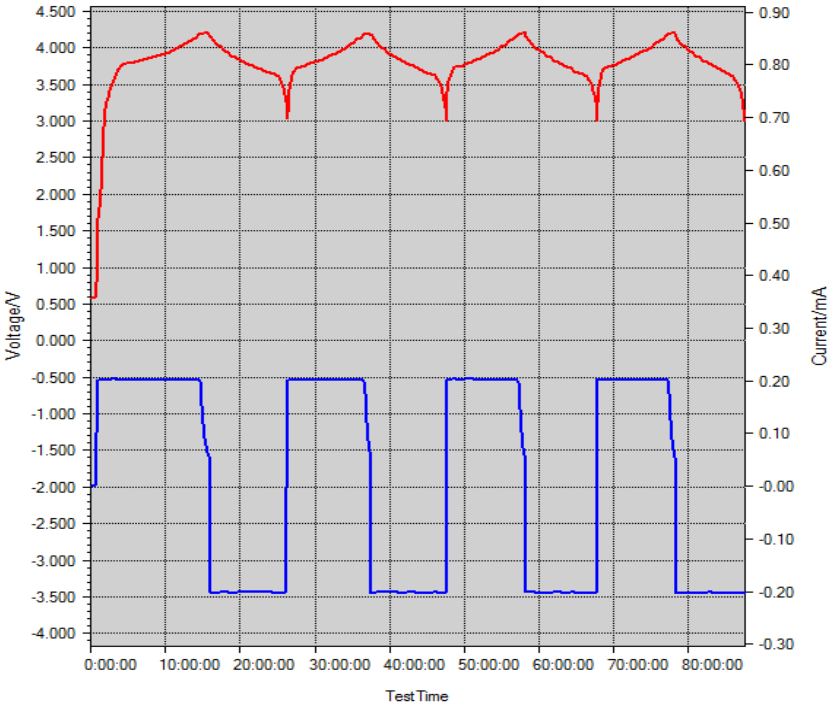

Figure 4.1. Charge-discharge characteristic of Full coin cell battery

Below table 10 shows the multiple charge-discharge cycle of a commercial lithium ion battery with an average efficiency of 80 percent was achieved and the battery was cycled for 20 cycles.

Table: 10 charge-discharge capacity of Full cell Battery

	Index	Charge-Ca...	Discharge-...	Efficienc...	Mid_Volt/V	CC-Percen...	FlatD/%
[-]	001	2.902	2.130	73.4	3.7692	96.3	87.3
[+]	0001 Rest			1:00:00	0.000	0.0	0.000
[+]	0002 Charge CC			13:48:38	2.794	0.0	10.483
[+]	0003 Charge CV			1:07:49	0.108	0.0	0.455
[+]	0004 Discharge CC			10:31:44	2.130	0.0	8.046
[-]	002	2.168	2.033	93.8	3.7739	96.3	86.0
[+]	0005 Charge CC			10:19:11	2.088	0.0	8.115
[+]	0006 Charge CV			0:48:25	0.080	0.0	0.335
[+]	0007 Discharge CC			10:02:41	2.033	0.0	7.674
[-]	003	2.057	1.956	95.1	3.7766	96.2	85.2
[+]	0008 Charge CC			9:46:23	1.978	0.0	7.697
[+]	0009 Charge CV			0:47:42	0.079	0.0	0.330
[+]	0010 Discharge CC			9:39:39	1.956	0.0	7.378
[-]	004	2.020	1.871	92.6	3.7746	95.9	83.1
[+]	0011 Charge CC			9:34:00	1.936	0.0	7.542
[+]	0012 Charge CV			0:51:34	0.084	0.0	0.352
[+]	0013 Discharge CC			9:14:16	1.871	0.0	7.043

4.1.2 Half-cell lithium ion battery

For the better understanding of a working half-cell battery, graphite based half-cell was fabricated. Figure 4.2 shows the charge-discharge cycle of a standard 40mAH rated coin cell lithium ion half-cell battery with a graphite electrode and was characterized using land CT2001A battery tester at the higher input current rate of 8mA. Charge and discharge was performed for multiple cycles and the maximum discharge capacity of 4.427 mAh in 6th cycle and Maximum charge capacity of 4.406 mAh in 7th cycle. The characteristic voltage plateaus near ~ 0.15 V for discharging and ~ 0.1 V for charging was observed which shows that graphite is a good candidate of anode material due to the charge-discharge potential difference between them.

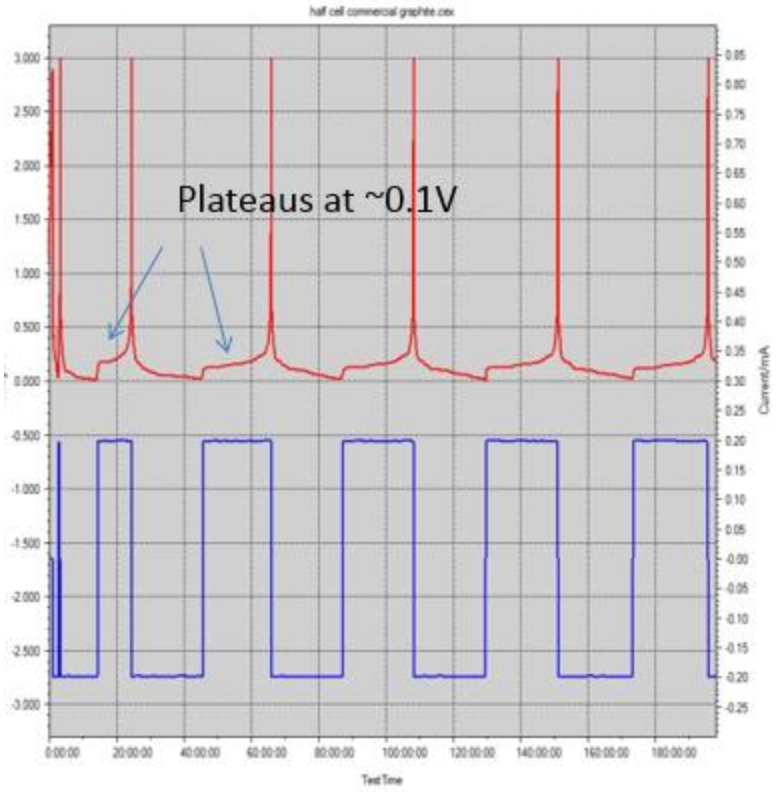

Figure 4.2. Charge-discharge characteristic of half coin cell battery

Table: 11 Charge-discharge capacity of Half-cell battery

	Index		Charge-Cap./mAh	Discharge-Cap./mAh	Efficiency/%	Mid_V
[-]	001		0.000	0.336	0.0	0.
	[+]	0001 Rest	1:00:00	0.000	0.0	
	[+]	0002 Discharge CC	1:41:44	0.336	0.0	
[-]	002		0.137	2.193	0.0	0.
	[+]	0003 Charge CC	0:41:32	0.137	0.0	
	[+]	0004 Discharge CC	11:03:54	2.193	0.0	
[-]	003		1.997	4.174	0.0	0.
	[+]	0005 Charge CC	10:04:52	1.997	0.0	
	[+]	0006 Discharge CC	21:03:52	4.174	0.0	
[-]	004		4.053	4.213	103.9	0.
	[+]	0007 Charge CC	20:27:26	4.053	0.0	
	[+]	0008 Discharge CC	21:15:29	4.213	0.0	
[-]	005		4.165	4.268	102.5	0.
	[+]	0009 Charge CC	21:01:32	4.165	0.0	
	[+]	0010 Discharge CC	21:31:15	4.268	0.0	
[-]	006		4.230	4.427	104.7	0.
	[+]	0011 Charge CC	21:20:52	4.230	0.0	
	[+]	0012 Discharge CC	22:21:05	4.427	0.0	
[-]	007		4.406	0.459	10.4	0.
	[+]	0013 Charge CC	22:14:28	4.406	0.0	
	[+]	0014 Discharge CC	2:19:00	0.459	0.0	

4.2 Anatase TiO2 as anode

4.2.1 Dektak Profilometer for thickness measurement

Figure 4.3 shows the dektak profilometer analysis of anatase TiO2 on copper foil. The thickness of anode material was measured in order to ensure efficient performance of the TiO2 based battery. Multiple layer doctor blading technique was used to achieve the thickness of ~60 micrometer and thickness profile was measures using a dektak profilometer.

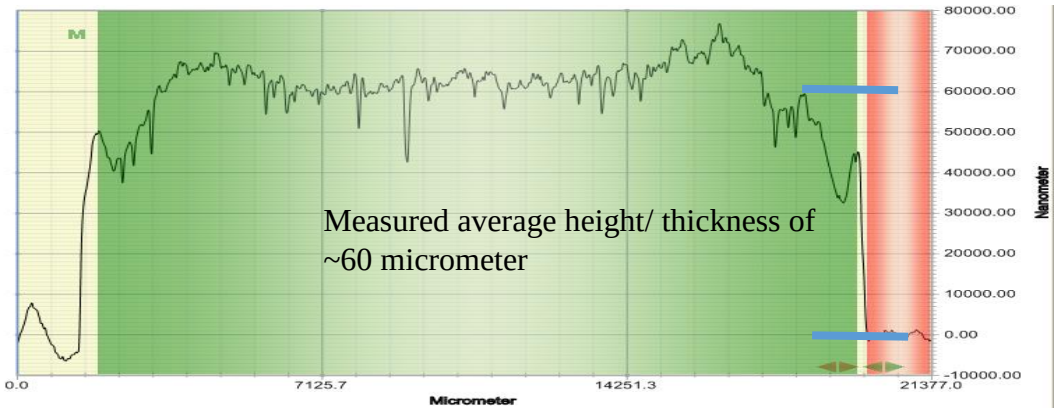

Figure 4.3. Thickness measurement of TiO2 anode

4.2.2. Scanning electron microscope (SEM) measurement for surface uniformity and roughness

Figure 4.4. shows the scanning electron microscopic (SEM) measurement of three layered doctor bladed TiO2 slurry (80:10:10) on a copper foil. Figure 4.4 (a) shows the 50 micrometer magnification of a dense layer anode material doctor bladed. The film relatively look uniform as it is important for proper lithiation and delithiation of lithium ions onto the electrode surface. Figure 4.4 (b) shows the 5 micrometer magnification in

which Minor defects was identified as the film was not controlled in a cleanroom environment.

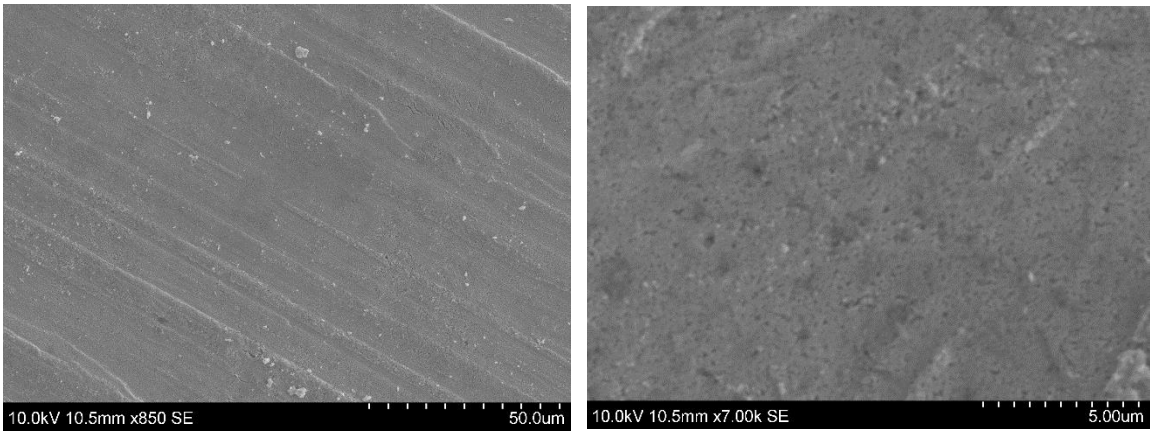

Figure 4.4. Scanning electron microscope (SEM) image of TiO2 based anode (a) 50 micrometer magnigication (b) 5 micrometer magnification

4.3 Charge-Discharge profile of TiO2 based battery

4.3.1 TiO_2 Half coin cell battery

Figure 4.5 shows the first and second cycles electrochenical charge-discharge profile of half cell TiO2 electrode. The voltage plateaus was identified near ~1.95 V for charging and ~1.8 V for discharging in which the potential difference between there plateaus make Anatase TiO2 a right candidate as a anode material for lithium ion full cell battery. The first cycle discharge capacity of 250 $mAhg^{-1}$ and charge capacity of 180 $mAhg^{-1}$ was observed. The theoritical capacity calculated was 330 $mAhg^{-1}$. The lower in practical capacity was however due to the presence of lithium greater than 0.5 in Li_xTiO_2 leads for better lithium-lithium intercalation. The columbic efficiency of ~80% was achieved which indicates good reversible capacity of the material the cycle was repeated for about 25 cycles and acceptable specific capacity of 135 $mAhg^{-1}$ was recorded.

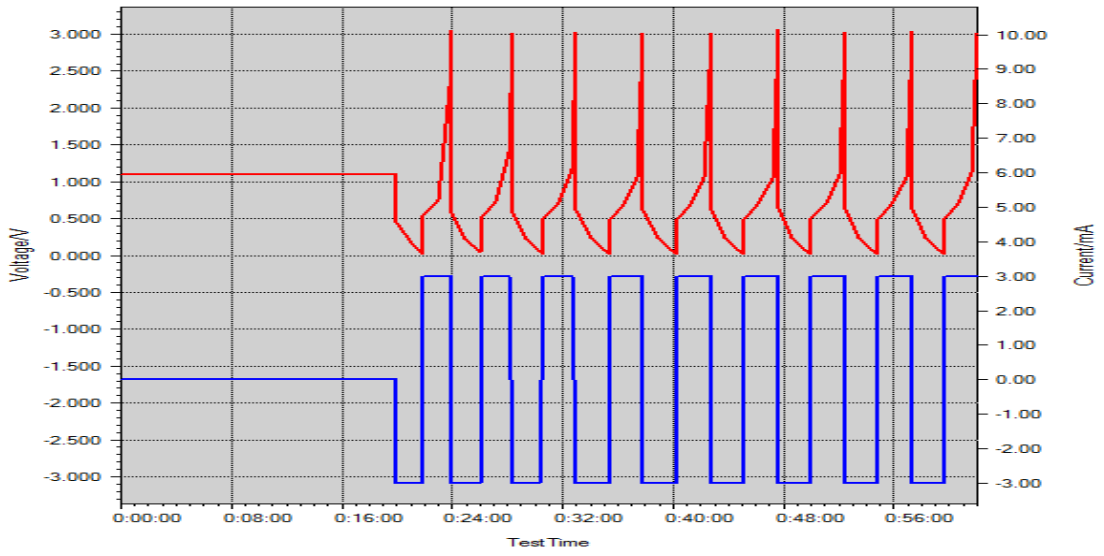

Figure 4.5. TiO2 Anatase Half-cell performance

4.3.2 TiO_2 Full coin cell battery

Figure 4.6 (a) and (b) shows the charge discharge capacity and coulombic efficiency performance of an Anatase TiO2 anode and LiCoO2 cathode full coin cell battery. The electrochemical charge discharge profile was recorded for 25 cycles. The reaction between the charge-discharge process was:

$$TiO_2 + LiCoO_2 \leftrightarrow Li_xTiO_2 + Li_{1-x}CoO_2$$

Figure 4.6 (a) represents that the full cell had acceptable reversible cyclability with the first cycle dicharge capacity of 0.7-0.9mAh and 0.8-1 mAh charge capacity was recoded which is comparable to the reported capacity of 1.2 mAh for discharge capacity and 1.4 mAh for charge capacity. Figure 4.6 (b) represents an coulombic effeciency achieved of about 90-94% for multiple charge-discharge cycle which shows stable behaviour of the electrodes.

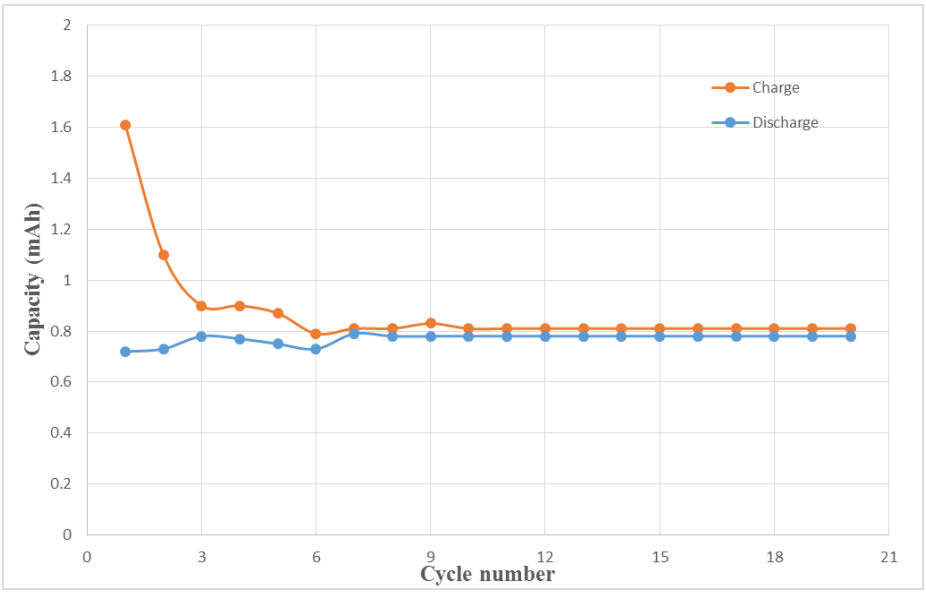

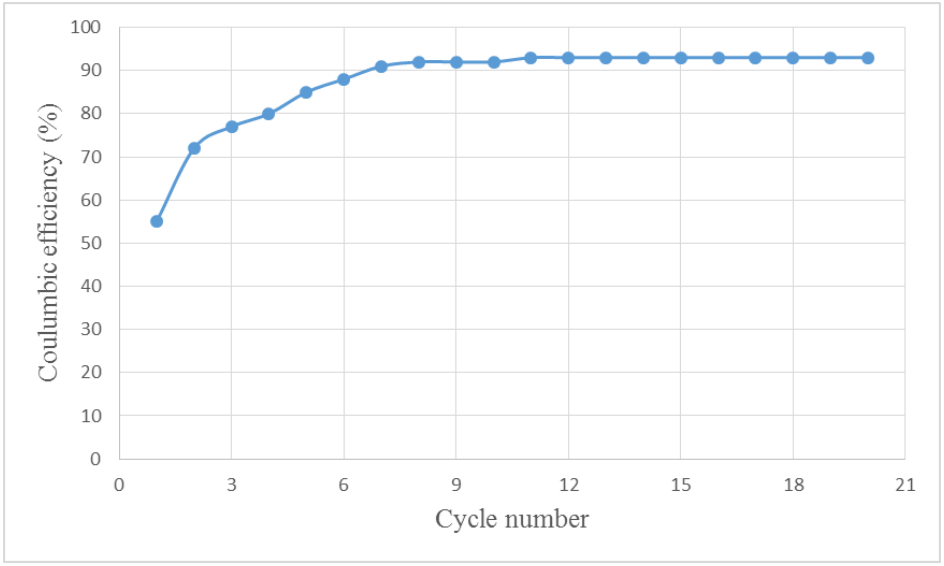

Figure 4.6 (a) charge-discharge capacity (b) Coulombic efficiency of a Full cell Anatase TiO2- LiCoO2 coin cell battery

4.3.3 TiO_2 Full thin film battery

Figure 4.7 shows the cycle capacity of Anatase TiO2 –LiCoO2 based lithium ion full coin cell battery. As the battery was cycled through multiple charge-discharge cycle

the common decrease in capacity was observed. The average capacity of 0.8 mAh was obtained for a slower discharge rate of C/10 and was able to recover the specific capacity even after 10 cycles which shows stable performance of the battery.

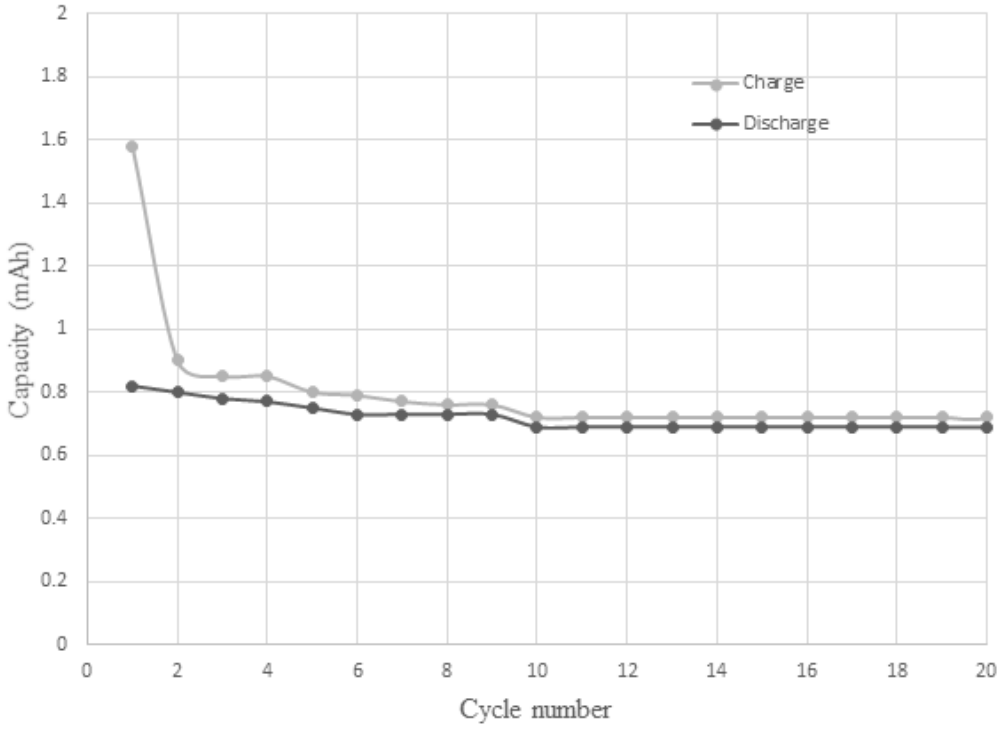

Figure 4.7 cycle capacity of Anatase TiO2 based lithium ion full cell thin film battery

4.4 Characterization of standard DSSC

4.4.1 Standard DSSC front and back illumination

Figure 4.8 shows the standard operation of DSSC. FTO substrate was used as a counter electrode and photo anode and was characterized front and rear illumination in order to evaluate its performance for integrated device as the integrated will have a rear illumination. Table… shows the performance of FTO and Ti based standard DSSC. The front illumination of ~6.5% efficiency and ~3% efficiency in the rear side. This low efficiency might be due to the low transmission of light due to the scattering layer. Hence,

the titanium based DSSC was characterized with and without scattering layer and light was illuminated at the rear side of the DSSC. With scattering layer only ~2% of efficiency was possible and with rear illumination an efficiency of ~3% was achieved hence this has a very low voltage and low efficiency which makes it very limited for integrated performance.

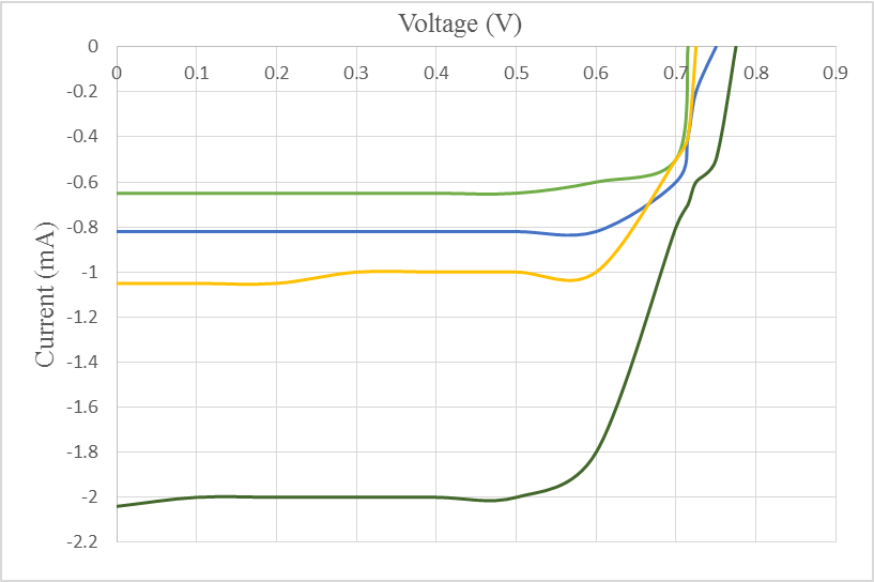

Figure.4.8 Characterization of DSSC of FTO and Ti foil with front and rear illumination

Hence, more transparent and high efficient DSSC was investigated by Pt/AZO treated counter electrode that can allow more light to pass through the counter electrode that can be used for the integrated pack.

Table.12 Performance of rear and front side illuminated DSSC

Sample	Illumination	Voc (V)	Jsc (mA/cm^2)	Power (mW)	FF	Efficiency(%)
FTO-DSC/with scattering layer	Front	0.775	11.9	0.92	0.67	6.18
FTO-DSC/with scattering layer	Back	0.76	6.87	0.52	0.7	3.65
Ti-DSC/with scattering layer	Back	0.715	4.08	0.29	0.71	2.07
Ti-DSC/without scattering layer	Back	0.725	5.93	0.43	0.69	2.97

4.4.2 Characterization of Pt and Pt/AZO treated DSSC

Figure 4.9 shows the Pt/AZO coated counter electrode DSSC characterization where Jsc (short circuit current density), Voc (Open circuit voltage) and form factor are recorded. In which the concentration on Pt and AZO ratio is mixed in ratio of (2:1) and light illumination at AM 1.5 light intensity 1000 $mWcm^{-2}$. The J-V curve shows demonstrated efficiency of 7.58% for Pt/AZO at (2:1) for the front illumination in which the results do not prove any significant difference in their performance compared to the standard DSSC.

Figure 4.10 shows the rear illumination characterization of Pt and Pt/AZO a demonstrated efficiency of 4.49 for Pt/AZO at (2:1). The highest concentration of Pt with (2:1) ratio has shown the significant improve in efficiency than the other concentration which shows a high Jsc as shown in the table 12. This is due to the more transparent counter electrode which allows light to pass through the dye. This results indicate that the use of Pt/AZO treated counter electrode helps in rear illumination application required for the Integrated DSSC with the battery.

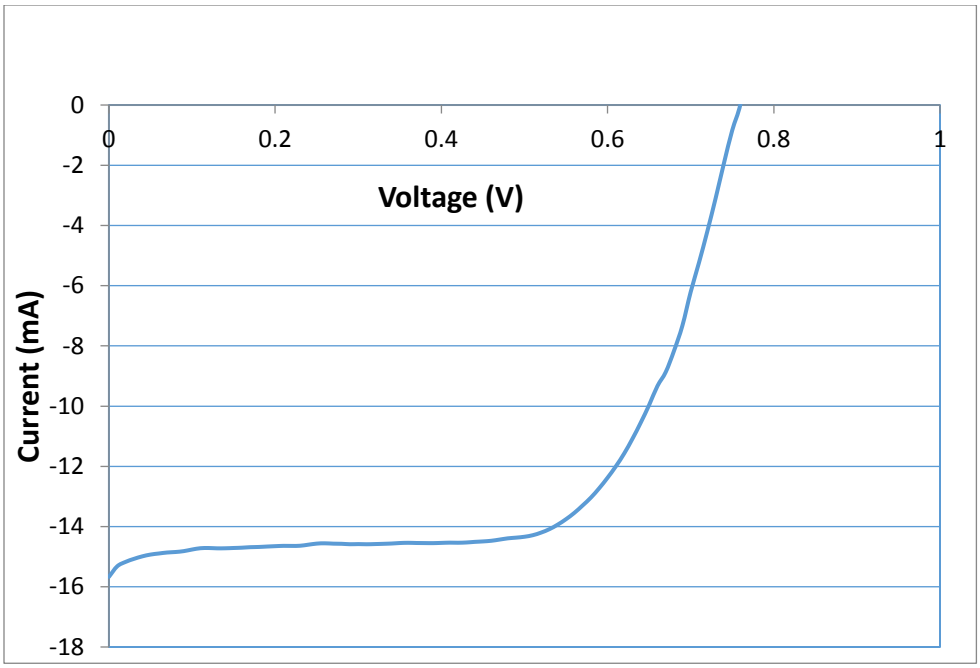

Figure.4.9: Current- voltage characterization of Pt/AZO (2:1) ratio Front solar illumination

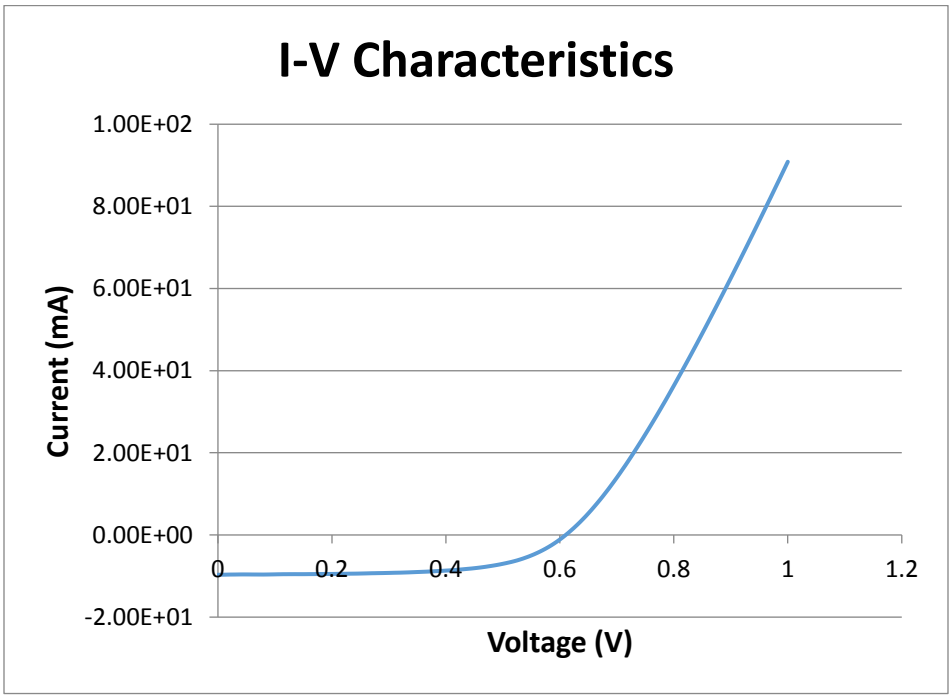

Figure.4.10: Current- voltage characterization Pt/AZO with (2:1) Rear solar illumination

Table 13: J-V performance Pt/AZO based DSSC with front and rear illumination

Parameters	Front illumination	Rear illumination
Voc	0.76	0.65
Jsc	-1.51E+01	-12.077875
Voc*Jsc	-11.45636	-7.85061875
Max Power	-7.5852	-4.49887375
Fill Factor	0.662095	0.573059767
Efficiency	7.5852	4.49887375

4.5 Characterization of commercial coin cell using dc power supply:

Figure 4.11 shows the charging profile of a 3V commercial full cell, battery charging using a boost convertor bq25504EVM. The battery was initially discharged to 2V using LAND CT2001A battery tester. The boost convertor was then connected to charge the discharged battery. A low voltage of 0.6 V was sufficient to charge the battery to 3.15V and the battery was successfully charged. The boost converter continued to maintain the charged battery voltage to 3.15 V by drawing current from dc supply when voltage goes down.

The following technique was used to charge the thin film battery integrated with DSSC to reduce the complexity of Tandem or complicated solar cell structures to charge the battery. This experiment proves that the external low voltage boost can sufficiently charge the battery.

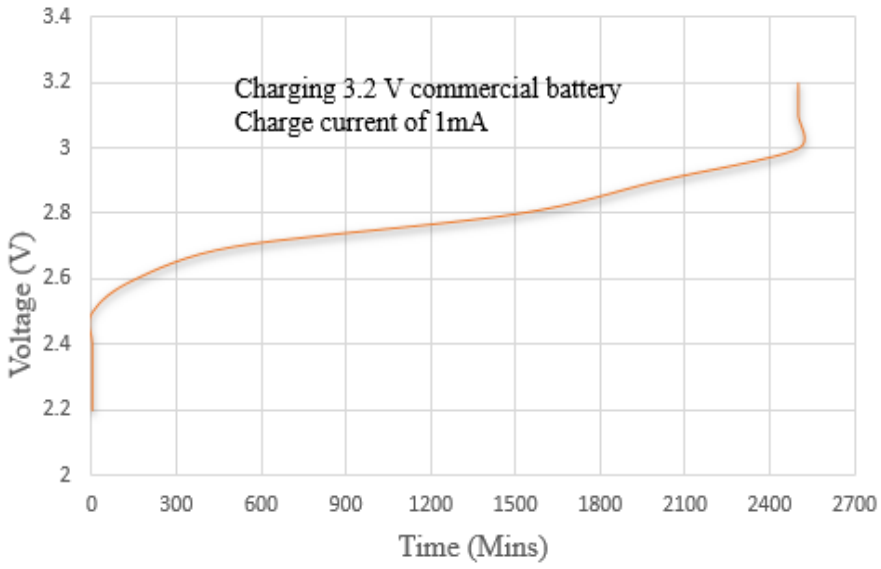

Figure 4.11 charging profile of commercial full cell battery using low voltage boost convertor.

4.6 Charge-discharge profile of Battery and solar cell

4.6.1 Independently charged coin cell battery using commercial silicon solar cell and Land tester without boost converter

Figure 4.12 shows the charge-discharge profile of commercial full cell battery using a series of CIS solar panels. The commercial battery was charged to around 3V using series of commercial solar cell. The variable in charge-discharge current was observed due to battery performing as a variable resistor in which a high/low current is observed with the low/high voltage variations at the input. As current is inversely proportional to the voltage the variation of power is always noticed with respect to the number of cycles in the battery performance.

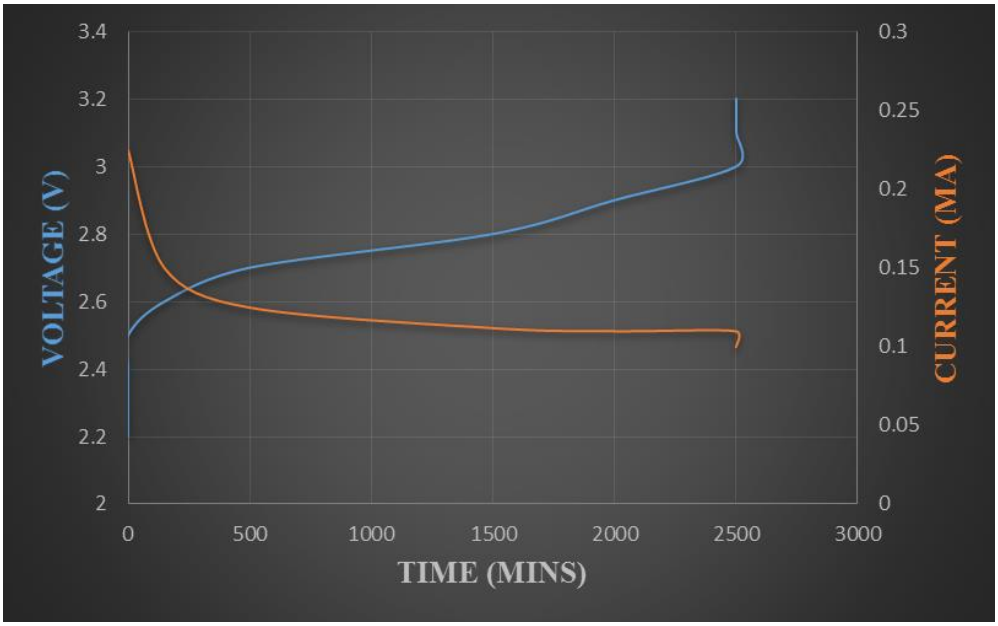

Figure 4.12 charge-discharge profile of commercial full cell battery using a series of solar panels.

4.6.2 Independently charged thin film battery using DSSC and Land tester

Commercial 3V full cell battery was charged using a Pt/AZO coated DSSC which was illuminated as the charging source and ultra-low power voltage boost convertor bq25504EVM. The battery was initially discharged to 2V using a LAND CT2001A battery tester. The battery was then charged using the DSSC source input in which the DSSC was charged under AM 1.5 100mWcm^{-2} of illumination. The DSSC during battery charging was comparable with the J-V output of the DSSC during characterization which is shown in the table below. Boost convertor was designed to operate at the 80% of Voc according to the data sheet of used chip. But the Voc/V_{PV} of DSSC was 76.9% which may be due to the voltage drop at the input of converter chip. The battery was then charged using

V_{in}=0.6V and Iin=100μA boost convertor and a comparable charging efficiency of ~80% was achieved.

Table 14: Maximum power point operation of DSSC using boost converter

	V_{PV} (V)	**I_{PV} (mA)**	**Power (mW)**
DSC during battery charging	0.567	0.67	0.38
IV curve MPP	0.621	0.632	0.392

Figure 4.13 shows the charging comparison of Land battery tester versus the DSSC charging using boost converter. The Land battery tester usually took less time on charge and discharging the battery which was around 15 minutes for one complete charge-discharge cycle. Whereas, DSSC took around 2 hours for complete first cycle charge and discharge profile and cycle time was drastically reduced to 15 minutes from sixth cycle.

Figure 4.14 shows the charge-discharge specific capacity with respect to number of cycles. Discharge capacity of 172 $mAhg^{-1}$ was seen at first cycle with the fading of discharge capacity over time and was consistent for ~45 to 55 $mAhg^{-1}$ for few cycles. The lower capacity might be due to the sealing issues in thin film battery between the electrodes. As the imperfect sealing leads to electrolyte exposure to air. At the end of 20 cycle energy storage efficiency was calculated for around 80% which is comparable to the previous recorded efficiency in Tandem DSSC Guo et al., [13] this was achieved without Tandem structure of DSSC but with a simple help of Boost converter chip.

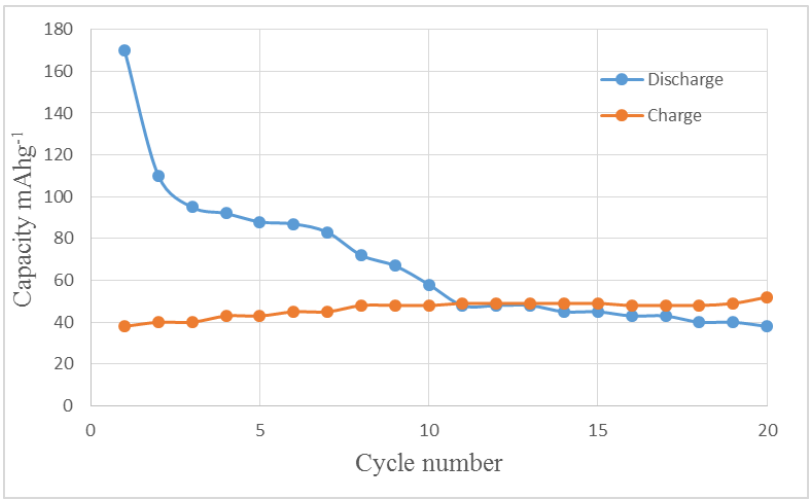

Figure 4.13 Characterization of independently charged-Discharge Battery using DSSC and boost convertor

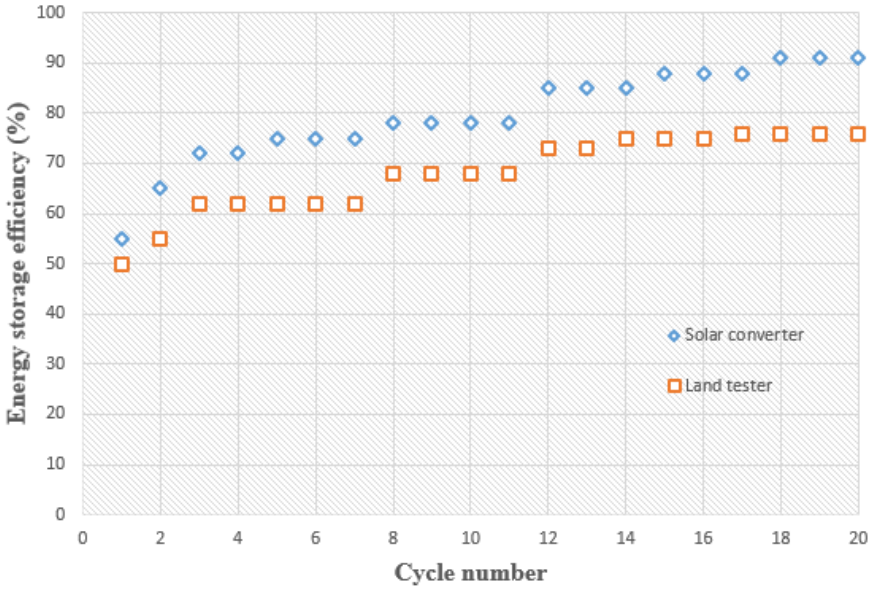

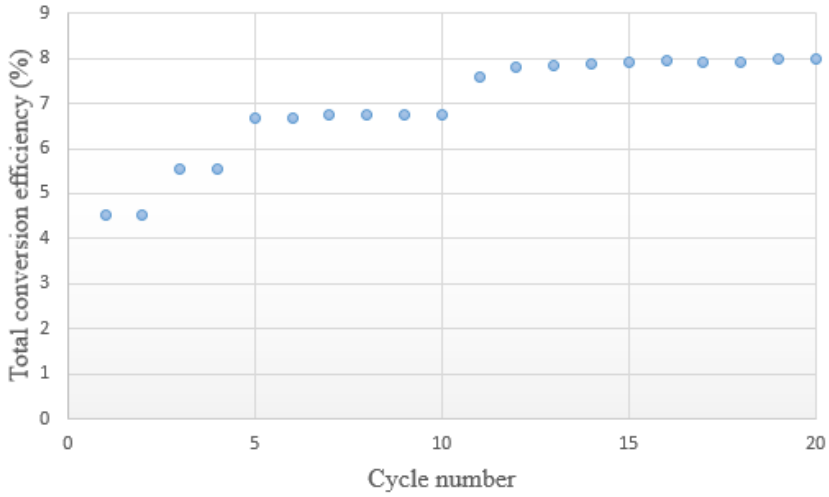

Figure 4.14 Efficiency of the converter based solar charging of coin cell independently

4.6.3 Integrated DSSC-Li-ion battery characterization

Figure 4.16 shows the Integrated DSSC- Lithium ion battery with a common titanium foil as an anode, charge discharge profile using the boost converter under different electric current density. With low input discharge current, higher and consistence specific capacity of ~40 to ~55 $mAhg^{-1}$ was observed at 20μA and capacity fading was observed as the discharge current was increased, this low capacity may be due to poor adhesion of epoxy to titanium foil which may lead to the electrolyte exposure to air. An average efficiency of 0.8% was achieved for around 20 cycles which was comparable to the TiO_2 based battery performance.

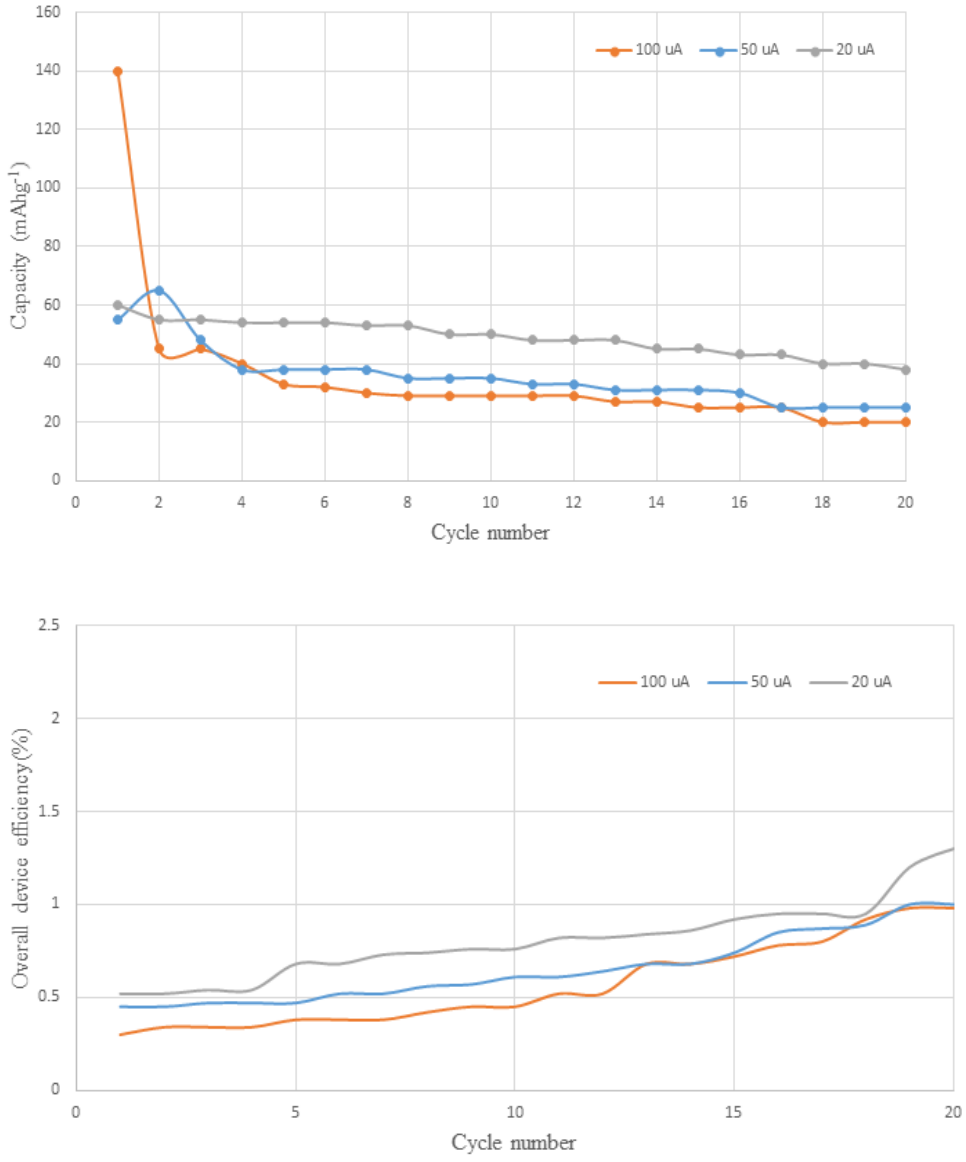

Figure 4.15 Performance of Integrated DSSC-Li-ion Battery

Chapter 5 : Conclusions

5.1 Summary

Energy harvesting been important technology concern to meet day to day energy requirements, due to growing population and automation industries. Consumption of fossil fuels such as coal, oil and natural gas leads to the emission of greenhouse gases which leads to global warming. Hence, a renewable energy source which is pollution free is required. Solar energy is being identified as abundant source of energy which is promising for energy harvesting.

Solar panels are addressed to gain more attention on energy consumption due to low cost and simplicity in operation. But energy storage had been a critical part due to inconsistency in solar illumination due to clouds, absence of sun light and difference in intensity. Hence, the battery storage was introduced to store the solar power. But, when solar panels need to be connected to huge battery systems and connecting series of solar panels to drive high voltage leading big consumption of space and complexity. Hence, a simple energy conversion system is important to store the solar power. Therefore, an approach was made to integrate a single solar cell with thin film battery which can demonstrate energy harvesting for mobile application.

Hence, an integrated power pack approach was made using organic type solar cell, Dye sensitized solar cell (DSSC) with platinum and Aluminum zinc oxide (Pt/AZO) modified counter electrode for more transparent rear illumination which had a power conversion efficiency of ~4.49% and anatase TiO_2 based lithium ion thin film battery using with a common Titanium foil substrate as an electrode between them and a low power

energy boost converter with V_{in}=0.6V and I_{in}=100μA was used for sufficient input voltage to charge the battery.

The battery was successfully charged for 20 cycles using this technique and an average efficiency of ~0.8% was recorded with average current energy density of 55$mAhg^{-1}$ was achieved with different discharge input current of 20 μA.

5.2 Conclusions

Single DSSC solar cell integrated with lithium ion battery using a common electrode with a low power energy boost converter demonstrated simplifying energy harvesting system for mobile application. Anatase TiO_2 material based thin film cell with a demonstrated current density of ~55 mAh for 20 cycles and Transparent counter electrode with a rear illumination with total power conversion efficiency of ~4.49%. Hence an integrated power pack of DSSC-Li ion battery was fabricated and characterized with charge-discharge profile of battery for 20 cycles with overall average efficiency of 0.8% with ~40$mAhg^{-1}$ of energy density.

5.3 Future Work

Better material selection to achieve enhanced overall conversion efficiency and storage need to be identified. There is need for better charge current density with more stable and longer cycle life of the battery need to be addressed for integrated device on enhancing the energy harvesting technology for mobile applications.

References

[1] Energy transitions: Past and Future- Prepared in Partnership with IHS CERA

[2] F. S. e. a. J.L. Sawin, "Renewables 2016- Global Status Report," REN212016.

[3] NASA global temperature record finder http://www.climatecentral.org/news/record-hot-temps-another-month-20715

[3] Energy Outlook Special Report 2016 energy and air pollution

[4]Wikipedia. (2015). Solar Energy. Available: http://en.wikipedia.org/wiki/Solar_energy

[5] D. M. Chapin, C. S. Fuller, and G. L. Pearson, "A New Silicon p-n Junction Photocell for Converting Solar Radiation into Electrical Power," Journal of Applied Physics, vol. 25, pp. 676-677, 1954.

[6] T. E. Hoff and R. Perez, "Quantifying PV power Output Variability," Solar Energy, vol. 84, pp. 1782-1793, 10// 2010.

[7] J. Marcos, O. Storkël, L. Marroyo, M. Garcia, and E. Lorenzo, "Storage requirements for PV power ramp-rate control," Solar Energy, vol. 99, pp. 28-35, 1// 2014.

[8] H. Ibrahim, A. Ilinca, and J. Perron, "Energy storage systems—Characteristics and comparisons," Renewable and Sustainable Energy Reviews, vol. 12, pp. 1221-1250, 6// 2008.

[9] W. Guo, X. Xue, S. Wang, C. Lin, and Z. L. Wang, "An Integrated Power Pack of Dye-Sensitized Solar Cell and Li Battery Based on Double-Sided TiO2 Nanotube Arrays," Nano Letters, vol. 12, pp. 2520-2523, 2012/05/09 2012.

[10] R. Muhida, A. Mostavan, W. Sujatmiko, M. Park, and K. Matsuura, "The 10 years operation of a PV-micro-hydro hybrid system in Taratak, Indonesia," Solar Energy Materials and Solar Cells, vol. 67, pp. 621-627, 3// 2001.

[11] B. O'regan and M. Grfitzeli, "A low-cost, high-efficiency solar cell based on dye-sensitized," nature, vol. 353, pp. 737-740, 1991.

[11] T. N. Murakami, N. Kawashima, and T. Miyasaka, "A high-voltage dye-sensitized photocapacitor of a three-electrode system," Chemical Communications, pp. 3346-3348, 2005.

[12] X. H. Xi Zhang, Chensha Li, and Hongrui Jiang, "Dye-Sensitized Solar Cell with Energy Storage Function through PVDF/ZnO Nanocomposite Counter Electrodes," Advanced Materials, vol. 25, pp. 4093-4096, 2013.

[13] W. Guo, X. Xue, S. Wang, C. Lin, and Z. L. Wang, "An Integrated Power Pack of Dye-Sensitized Solar Cell and Li Battery Based on Double-Sided TiO2 Nanotube Arrays," Nano Letters, vol. 12, pp. 2520-2523, 2012/05/09 2012.

[14] Z. Yang, L. Li, Y. Luo, R. He, L. Qiu, H. Lin, et al., "An integrated device for both photoelectric conversion and energy storage based on free-standing and aligned carbon nanotube film," Journal of Materials Chemistry A, vol. 1, pp. 954-958, 2013.

[15] C. H. a. S. Bowden. (04/09/2015). PN Junction. Available: http://pveducation.org/pvcdrom/pn-junction/diffusion

[16] S. O. Kasap, "Solar Cells," in Principles of Electronic Materials and Devices. vol. 3rd edition, ed: New York: McGraw Hill, 2006.

[17] J. Nelson, the Physics of Solar Cells. London: Imperial College Press, 2003.

[18]C. Longo and M.-A. De Paoli, "Dye-sensitized solar cells: a successful combination of materials," Journal of the Brazilian Chemical Society, vol. 14, pp. 898-901, 2003.

[19] S. A. Haque, E. Palomares, B. M. Cho, A. N. Green, N. Hirata, D. R. Klug, et al., "Charge separation versus recombination in dye-sensitized nanocrystalline solar cells: the minimization of kinetic redundancy," Journal of the American Chemical Society, vol. 127, pp. 3456-3462, 2005.

[20] U.S. Energy Information Administration, based on Energy Storage Association.

[21] Philipp Adelhelm From lithium to sodium: cell chemistry of room temperature sodium–air and sodium–sulfur batteries

[22] Y. Brunet, Energy Storage,, ISTE Ltd 2011 Battery university- types of lithium ion battery

[23] B. Scrosati and J. Garche, "Lithium batteries: Status, prospects and future," Journal of Power Sources, vol. 195, pp. 2419-2430, 5/1/ 2010.

[24] T. J. Patey, "Oxide Nanoparticles for Electrodes in Lithium-Ion Batteries," Doctor of Sciences, ETH ZURICH, 2009.

[25]Y. Yao, "Carbon based anode materials for lithium-ion batteries," Master of Materials Engineering, University of Wollongong, 2003.

[26] W. Guo, X. Xue, S. Wang, C. Lin, and Z. L. Wang, "An Integrated Power Pack of Dye-Sensitized Solar Cell and Li Battery Based on Double-Sided TiO2 Nanotube Arrays," Nano Letters, vol. 12, pp. 2520-2523, 2012/05/09 2012.

[27] H. Hoppe and N. S. Sariciftci, "Organic solar cells: An overview," Journal of Materials Research, vol. 19, pp. 1924-1945, 2004.

[28] Y. Yao, "Carbon based anode materials for lithium-ion batteries," Master of Materials Engineering, University of Wollongong, 2003.

[29] T. J. Patey, "Oxide Nanoparticles for Electrodes in Lithium-Ion Batteries," Doctor of Sciences, ETH ZURICH, 2009.

[30] P. Tiwari, "Integration of Photovoltaics with Micro-Hydro Power Systems," Master of Science, Electrical Engineering, South Dakota State University, 2014.

[31] S. Dhakal, "Spatially diverse photovoltaic power plants for reduced power and voltage fluctuation using weather forecast," Master of Science, Electrical Engineering, South Dakota State University, 2013.

[32] M. Grätzel, "Conversion of sunlight to electric power by nanocrystalline dye sensitized solar cells," Journal of Photochemistry and Photobiology A: Chemistry, vol. 164, pp. 3-14, 6/1/ 2004.

[33] N.-G. Park and K. Kim, "Transparent solar cells based on dye-sensitized nanocrystalline semiconductors," physica status solidi (a), vol. 205, pp. 1895-1904, 2008.

[34] B. A. Gregg, F. Pichot, S. Ferrere, and C. L. Fields, "Interfacial Recombination Processes in Dye-Sensitized Solar Cells and Methods To Passivate the Interfaces," The Journal of Physical Chemistry B, vol. 105, pp. 1422-1429, 2001/02/01 2001.

[35] M. Yu, X. Ren, L. Ma, and Y. Wu, "Integrating a redox-coupled dye-sensitized photoelectrode into a lithium–oxygen battery for photoassisted charging," Nat Commun, vol. 5, 10/03/online 2014.

[36] C. J. H. D.T. Ton, G. H. Peek and J. D. Boyes, "Solar Energy Grid Integration Systems-Energy Storage (SEGIS-ES)," Sandia National Laboratories2008.

[37] P. J. Hall and E. J. Bain, "Energy-storage technologies and electricity generation," Energy Policy, vol. 36, pp. 4352-4355, 12// 2008.

[38] H.-W. Chen, C.-Y. Hsu, J.-G. Chen, K.-M. Lee, C.-C. Wang, K.-C. Huang, et al., "Plastic dye-sensitized photo-supercapacitor using electrophoretic deposition and compression methods," Journal of Power Sources, vol. 195, pp. 6225-6231, 9/15/ 2010.